HHS Public Access

Author manuscript

Nat Immunol. Author manuscript; available in PMC 2019 April 15.

Published in final edited form as:

Nat Immunol. 2018 November ; 19(11): 1212–1223. doi:10.1038/s41590-018-0232-x.

Fibrin-targeting immunotherapy protects against neuroinflammation and neurodegeneration

Jae Kyu Ryu[1], **Victoria A. Rafalski**[#1], **Anke Meyer-Franke**[#1], **Ryan A. Adams**[2], **Suresh B. Poda**[3], **Pamela E. Rios Coronado**[1], **Lars Østergaard Pedersen**[4], **Veena Menon**[3], **Kim M. Baeten**[1], **Shoana L. Sikorski**[2], **Catherine Bedard**[1], **Kristina Hanspers**[1], **Sophia Bardehle**[1], **Andrew S. Mendiola**[1], **Dimitrios Davalos**[1,12], **Michael R. Machado**[1], **Justin P. Chan**[1], **Ioanna Plastira**[1,5], **Mark A. Petersen**[1,6], **Samuel J. Pfaff**[7], **Kenny K. Ang**[7], **Kenneth K. Hallenbeck**[7], **Catriona Syme**[1], **Hiroyuki Hakozaki**[8], **Mark H. Ellisman**[8,9], **Raymond A. Swanson**[10,11], **Scott S. Zamvil**[11], **Michelle R. Arkin**[7], **Stevin H. Zorn**[3], **Alexander R. Pico**[1], **Lennart Mucke**[1,11], **Stephen B. Freedman**[1], **Jeffrey B. Stavenhagen**[4], **Robert B. Nelson**[3], and **Katerina Akassoglou**[1,2,11,*]

[1]Gladstone Institutes, San Francisco, California, USA.

[2]Department of Pharmacology, University of California, San Diego, La Jolla, California, USA.

[3]Lundbeck Research USA, Paramus, NJ, USA.

[4]H. Lundbeck A/S, 2500 Valby, Copenhagen, Denmark.

[5]Institute of Molecular Biology and Biochemistry, Medical University Graz, Austria.

[6]Division of Neonatology, Department of Pediatrics, University of California, San Francisco, San Francisco, California, USA.

* kakassoglou@gladstone.ucsf.edu. **Correspondence and requests for materials** should be addressed to K.A.
Present address: Department of Neurosciences, Lerner Research Institute, Cleveland Clinic Foundation, Cleveland, OH USA.

Author Contributions

J.K.R. performed and designed experiments and analyzed data. V.A.R. did two-photon imaging and AD studies. R.A.A., J.B.S., and R.B.N. produced antibodies. R.A.A., C.B., and S.L.S. did EAE experiments. D.D. performed EAE studies, A.M.F. and K.K.A. did microglia inhibition experiments. A.M.F., S.B.P., L.O.P., and V.M. and C.B. did antibody binding ELISA. K.M.B. did immunohistochemistry and coagulation assays. M.R.M. and P.E.R.C. did histology. I.P. performed immunoblots. A.S.M. performed qPCR array and flow cytometry. S.B., J.P.C., M.A.P, M.R.M. and P.E.R.C. did image analysis. S.J.P. and K.K.H. produced recombinant CD11b I domain. C.S., M.R.A., M.H.E., H.H, and R.B.N. analyzed data. K.H. and A.R.P. performed the bioinfomatics analysis. R.A.S., S.S.Z., S.H.Z., L.M., and S.B.F. designed experiments. J.B.S. and R.B.N. designed experiments and analyzed data. K.A. conceived the project, designed the study, and analyzed data. K.A. and J.K.R. wrote the manuscript with input from all authors.

Competing Interests

The authors declare competing financial interests.

Additional information

Supplementary Information accompanies this paper and includes nine Supplementary Figures and three Supplementary Tables.

Reporting Summary. Further information on research design is available in the Nature research Reporting Summary linked to this article.

Data Availability. GEO data supporting the findings of this study have been deposited in the GEO depository under accession numbers GSE118920 and GSE118921. Networks are permanently referenced in two Wikipathways entries http://wikipathways.org/index.php?title=Pathway:WP3625&oldid=85694, http://wikipathways.org/index.php?title=Pathway:WP3626&oldid=85691. The authors declare that all other data supporting the findings of this study are available within the paper. Any additional data can be made available from the corresponding author upon request.

[7]Small Molecule Discovery Center, Department of Pharmaceutical Chemistry, University of California, San Francisco, San Francisco, California, USA.

[8]National Center for Microscopy and Imaging Research, University of California, San Diego, La Jolla, CA USA.

[9]Department of Neurosciences, University of California, San Diego, La Jolla, CAUSA.

[10]Neurology Service, San Francisco Veteran Affairs Medical Center, 4150 Clement St., San Francisco, CA, USA.

[11]Department of Neurology, University of California, San Francisco, San Francisco, California, USA.

[#] These authors contributed equally to this work.

Abstract

Activation of innate immunity and deposition of blood-derived fibrin in the central nervous system (CNS) occur in autoimmune and neurodegenerative diseases, including multiple sclerosis (MS) and Alzheimer's disease (AD). However, mechanisms linking blood-brain barrier (BBB) disruption with neurodegeneration are poorly understood, and exploration of fibrin as a therapeutic target has been limited by its beneficial clotting functions. Here we report the generation of monoclonal antibody 5B8 targeted against the cryptic fibrin epitope $\gamma_{377–395}$ to selectively inhibit fibrin-induced inflammation and oxidative stress without interfering with clotting. 5B8 suppressed fibrin-induced nicotinamide adenine dinucleotide phosphate (NADPH) oxidase and proinflammatory gene expression. In animal models of MS and AD, 5B8 entered the CNS and bound to parenchymal fibrin, and its therapeutic administration reduced innate immune activation and neurodegeneration. Thus, fibrin-targeting immunotherapy inhibits autoimmune- and amyloid-driven neurotoxicity and may have clinical benefit without globally suppressing innate immunity or interfering with coagulation in diverse neurological diseases.

Activation of innate immunity is a key feature of neurological diseases with different etiologies, including autoimmune and neurodegenerative CNS diseases[1]. Increasing evidence indicates that pathogenic activation of CNS innate immunity contributes to neuronal damage and modulates the onset and progression of neurodegenerative diseases[2]. Oxidative injury and release of free radicals have been proposed as common mechanisms for innate immune-driven neurodegeneration and demyelination in MS and AD[3–6]. Chronic innate immune activation and oxidative injury are key elements driving neurodegeneration in both relapsing-remitting– and progressive MS[3,7,8]. In progressive MS, there is robust microglia activation, oxidative stress, and neurodegeneration[3,8,9]. Pathogenic activation of innate immunity contributes to oxidative stress and cognitive decline in AD[5]. Little is known about the pathogenic signals that activate innate immune cells toward neurotoxic phenotypes. Understanding the mechanisms of activation of CNS innate immunity is essential for deciphering how neuroinflammation contributes to neuronal damage and for designing treatments for selective suppression of pathogenic functions of innate immunity.

Innate immune activation, blood-brain barrier (BBB) disruption, and fibrin deposition are intimately linked in neurological diseases[10,11]. The blood coagulation factor fibrinogen

extravasates into the CNS parenchyma upon BBB disruption and is converted to insoluble fibrin, a key proinflammatory matrix that activates innate immune responses[11,12]. Conversion of fibrinogen into fibrin exposes amino acids 377–395 in the fibrinogen γ chain ($\gamma_{377–395}$) that bind to the CD11b I-domain of complement receptor 3 (CR3) (also known as CD11b/CD18, Mac-1, $\alpha_M\beta_2$) and induces microglia and macrophage activation[13–16]. Fibrin is deposited in AD and MS lesions at sites of microglial activation and macrophage infiltration (reviewed in[11]). Fibrin is detected in progressive MS and in active and chronic lesions (reviewed in[11]). In progressive MS, fibrin deposition in the cortex correlates with neuronal loss and inhibition of fibrinolysis[17]. BBB disruption and fibrin deposition occur also early in MS and precede demyelination[18,19]. Fibrinogen has been proposed as a cerebrospinal fluid and plasma biomarker for AD and mild cognitive impairment, and increased fibrinogen concentrations are considered a predictor of brain atrophy in AD (reviewed in[11,20]). Depletion of fibrin either genetically in fibrinogen deficient mice or by anticoagulants decreases neuroinflammation, demyelination, and axonal damage in animal models of MS and reduces microglia activation, white matter damage, and cognitive decline in animal models of AD (reviewed in[11]). Fibrin induces rapid and sustained microglia responses and macrophage infiltration into the CNS[15,16]. Although increased BBB disruption and fibrin deposition correlate with neurodegeneration, the molecular links between blood leakage into the CNS and neuronal damage are poorly understood. Furthermore, whether and how fibrin-induced activation of innate immunity is neurotoxic remains largely unknown.

Here we report an unanticipated role for fibrin as an activator of the NADPH oxidase complex that induced reactive oxygen species (ROS) release and innate immune-driven neurotoxicity in autoimmune and amyloid-driven neurodegeneration. Although innate immune activation is an attractive candidate for therapeutic intervention, selective therapies to inhibit neurotoxic effects of innate immune responses are not widely available. By targeting the $\gamma_{377–395}$ cryptic fibrin epitope, we developed the first fibrin immunotherapy (monoclonal antibody 5B8) to selectively target the inflammatory form of fibrin without interfering with clotting or activation of innate immune cells by other ligands, such as lipopolysaccharide (LPS). 5B8 selectively bound to fibrin, but not soluble fibrinogen, and inhibited binding of fibrin to CR3 without interfering with fibrin polymerization, in vivo clotting time, or partial thromboplastin time (aPTT) in human plasma. 5B8 reduced NADPH oxidase activation, ROS release, microglial activation, and neurodegeneration in MS and AD animal models. These studies identify fibrin as a blood-derived signal that activates NADPH oxidase to promote innate immune-driven neurotoxicity, and identify fibrin-targeted immunotherapy as a novel therapeutic strategy to suppress innate immune-driven neurodegeneration at sites of increased vascular permeability without interfering with clotting or globally suppressing innate immunity.

Results

Design of fibrin-targeting immunotherapy.

The C- terminus of the fibrinogen γ chain contains two distinct non-overlapping sites at $\gamma_{400–411}$ and $\gamma_{377–395}$, which mediate platelet engagement and inflammation respectively

(Fig. 1a). Peptide $\gamma_{400–411}$ is the binding site for the platelet $\alpha_{IIb}\beta_3$ integrin receptor and is required for platelet aggregation. Peptide $\gamma_{377–395}$ is the binding site for the CD11b I-domain of CD11b/CD18[14] and is required for fibrin-induced activation of microglia and macrophages[13,15,16]. The $\gamma_{377–395}$ binding site is considered "cryptic" in the soluble fibrinogen molecule and is exposed only upon conversion of fibrinogen to insoluble fibrin[14] (Fig. 1a). We hypothesized that monoclonal antibodies against $\gamma_{377–395}$ would selectively recognize fibrin and inhibit fibrin's interaction with the CD11b I-domain without affecting blood coagulation. To control for CD11b I-domain binding specificity, we also generated mouse monoclonal antibodies against the $\gamma_{190–202}$ fibrin epitope, which is also cryptic, but is not required for binding to the CD11b I-domain[14]. Using a streamlined screening strategy, we selected monoclonal antibodies that selectively bind fibrin and inhibit microglia activation (Supplementary Fig. 1a). Antibodies 5B8, 4E11, and 4F1 had the highest selectivity and specificity for $\gamma_{377–395}$, while anti-$\gamma_{190–202}$ 1E3 did not bind $\gamma_{377–395,}$ as expected (Fig. 1b, Supplementary Fig. 1b). To discriminate between fibrinogen and fibrin in biochemical and cellular assays, we developed an *in vitro* fibrin substrate that binds to recombinant CD11b I-domain more strongly than fibrinogen (Supplementary Fig. 1c), suggesting $\gamma_{377–395}$ epitope exposure *in vitro*. All antibodies against cryptic epitopes bound with higher affinity to fibrin than to fibrinogen; among antibodies targeting $\gamma_{377–395}$, 5B8 bound fibrin to the greatest degree with minimal binding to soluble fibrinogen (Fig. 1c, Supplementary Fig. 1d). Competitive binding assays showed that 5B8 bound to human and mouse $\gamma_{377–395}$ peptides, but not $\gamma_{190–202}$ peptide (Supplementary Fig. 1e). 5B8 inhibited binding of the CD11b I-domain to fibrin (Fig. 1d), suggesting that 5B8 interferes with the ligand–receptor interaction.

Fibrin activates microglia, as evidenced by morphologic activation characterized by increase in cell size that is also associated with gene expression changes[13,16]. The morphologic activation assay, combined with automated quantification, was suitable for an unbiased and rapid comparison of multiple fibrin antibody clones in primary microglia cultures. Notably, among all antibodies generated against cryptic epitopes, only antibodies against $\gamma_{377–395}$ inhibited fibrin-induced morphologic activation of microglia; the highest inhibition (~87%) was by 5B8 (Supplementary Fig. 2a). The anti-$\gamma_{190–202}$ 1E3 antibody also bound fibrin but did not inhibit microglial activation (Supplementary Fig. 2a), suggesting that $\gamma_{377–395}$ must be targeted to inhibit fibrin's proinflammatory functions. The F(ab) fragment of 5B8 also inhibited fibrin-induced microglial activation (Supplementary Fig. 2b). 5B8 inhibited fibrin-induced morphologic microglial activation in a concentration-dependent manner and reduced proinflammatory gene expression (Fig. 1e, Supplementary Fig. 2c,d). Isotype control IgG2b with endotoxin concentrations <0.002 EU/μg (Supplementary Figs. 2e) was used as control for all experiments in the study. 5B8 did not alter the polymerization time of fibrinogen to fibrin, did not inhibit activated aPTT in human plasma, and had no effect on murine plasma clotting time in vivo (Fig. 1f-h). ~80% of 5B8 was recovered 5 days after a single intraperitoneal (i.p.) injection into healthy wild-type mice (Supplementary Fig. 2f), suggesting that 5B8's preferential binding to fibrin and minimal binding to soluble fibrinogen result in a minimal "sink-effect".

In microglia and macrophages, fibrin induces proinflammatory gene expression associated with immune response and cell recruitment[16]. In bone marrow derived macrophages

(BMDMs), 5B8 reduced fibrin-induced transcriptional activation of genes related to immune cell migration, adhesion, inflammatory responses, regulation of T cell proliferation, and chemotaxis, as shown by whole-genome microarray and Gene Ontology (GO) analysis (Fig. 2a-c). A heat map of the top 20 most affected transcripts showed that 5B8 inhibits fibrin-induced transcription of a group of genes that regulate innate/adaptive immune responses (Fig. 2c). Reductions in the expression of *Ccl24*, *Tnfs18*, *Il12b*, *Cxcl3*, and *Ifng* by 5B8 were validated by quantitative RT-PCR (Fig. 2d). 5B8 did not affect LPS-induced expression of proinflammatory genes (Fig. 2e), suggesting that the suppression of innate immune activation by 5B8 may be selective for fibrin. Further, 5B8 or its F(ab) fragment alone inhibited microglial activation and chemokine gene expression in fibrinogen-induced encephalomyelitis (Supplementary Fig. 3), an acute neuroinflammatory model resulting from fibrin-induced microglial activation[16]. Thus, we have devised a paradigm to develop a fibrin epitope-specific immunotherapy. The result is 5B8, a highly selective monoclonal antibody that blocks fibrin-induced, CD11b-mediated activation of innate immunity without affecting fibrin polymerization, in vivo clotting time, or aPTT in human plasma.

Fibrin induces NADPH oxidase-mediated neurodegeneration.

A consequence of activation of innate immunity in CNS autoimmune and neurodegenerative diseases is neurotoxicity, its successful treatment remaining a major unmet clinical need. Intriguingly, fibrin induced expression of several genes that regulate oxidative stress and ROS release (Fig. 3a) and that are implicated in neurotoxicity[7,21]. *Ncf4*, the gene that encodes the $p40^{phox}$ subunit of the NADPH oxidase Nox2 complex, was among the highest fibrin-upregulated genes (Fig. 3a). NADPH oxidase is a multicomponent enzyme system upregulated in human MS[22] and AD[23]. Increased NADPH-oxidase activation and oxidative stress are common mechanisms of neurodegeneration in diseases with fibrin deposition, including MS, AD, stroke, traumatic brain injury, and brain aging[6,24,25]. Intriguingly, fibrin increased protein expression of the Nox2 component $gp91^{phox}$, phosphorylation of $p40^{phox}$, and NADPH oxidase activity; these increases were all reduced when macrophages were treated with 5B8 (Fig. 3b,c). 5B8 treatment inhibited fibrin-induced ROS release in both mouse and human macrophages (Fig. 3d,e). Fibrin-induced ROS generation was reduced in BMDMs when the $p47^{phox}$ subunit of NADPH oxidase was ablated genetically ($p47^{phox-/-}$) and when NADPH-oxidase and CD11b were inhibited by treatment with apocynin or the anti-CD11b antibody M1/70, respectively (Fig. 3f,g and Supplementary Fig. 4a). In the culture conditions tested, fibrin stimulation or treatment with antibodies did not affect BMDM cell density (Supplementary Fig. 4b). In a co-culture of cortical neurons and macrophages, which recapitulates the non-cell-autonomous degeneration of CNS neurons, fibrin-primed macrophages induced significant loss of $MAP\text{-}2^{+}$ neurons and increased fragmentation and blebbing of neurites (Fig. 3h). Notably, 5B8 effectively blocked this pathogenic cascade (Fig. 3h). These results suggest that fibrin causes neurotoxicity via a causal chain that involves CD11b-mediated innate immune cell activation and increased ROS production by NADPH oxidase.

Fibrin immunotherapy protects from axonal damage in EAE.

Evidence from human MS has underscored the contributions of fibrin, innate immunity, and oxidative stress to disease onset, progression, and disability[3,8,9,19,22,26]. To examine the role

of fibrin on neurotoxicity in vivo, we first tested the effects of 5B8 in three experimental autoimmune encephalomyelitis (EAE) models that simulate key aspects of MS: relapsing-remitting $PLP_{139–151}$ EAE, chronic $MOG_{35–55}$ EAE, and adoptive transfer of $CD4^+$ T cells differentiated under T_H1-polarizing conditions. Given prophylactically, 5B8 reduced neurologic signs in all three models compared to IgG2b isotype control (Fig. 4a). Given prophylactically, 5B8 reduced the mean maximum clinical score and delayed the first day of onset as compared to the IgG2b-injected control groups (Supplementary Tables 1, 2). Given therapeutically, 5B8 reduced the severity of relapses in $PLP_{139–151}$ EAE (Fig. 4b, Supplementary Table 1). In all EAE treatment groups, 5B8 reduced the percentage of paralyzed mice (Fig. 4c). Fibrin is a cross-linked polymer of fibrinogen molecules. Consequently, anti-fibrinogen antibodies detect both fibrinogen and fibrin[11]. Fibrinogen is converted to fibrin at sites of increased coagulation activity[11]. In EAE spinal cord, coagulation activity promotes the conversion of fibrinogen to fibrin, leading to parenchymal fibrin deposition at areas of microglia activation and demyelination[27]. After i.p. injection of biotinylated 5B8 in mice with EAE, 5B8 spatially correlated with fibrin(ogen)-rich areas in the spinal cord (Fig. 4d), demonstrating target engagement.

To determine whether 5B8 inhibits inflammatory cell recruitment into the CNS, we treated after induction of EAE in *Cx3cr1*$^{GFP/+}$*Ccr2*$^{RFP/+}$ mice. 5B8 inhibited both the accumulation of $Cx3cr1^+$ microglia and the infiltration of $Ccr2^+$ monocytes into the CNS (Fig. 5). Increased NADPH oxidase activity and excessive ROS production are implicated in MS[28], and ROS generated by invading and resident CNS macrophages mediate demyelination and axonal damage in EAE[7]. 5B8 markedly reduced axonal damage, ROS generation, inflammation, and demyelination in EAE (Fig. 5, Supplementary Fig. 5a,b). In accordance with prior studies[7,12], axonal damage correlated with ROS^+ areas in EAE lesions (Supplementary Fig. 5c). The fibrin $\gamma_{377–395}$ peptide inhibits binding of fibrin to CD11b and suppresses EAE without affecting peripheral T cell responses[13]. Similarly, 5B8 did not significantly alter peripheral T cell responses in $PLP_{139–151}$ EAE mice (Supplementary Fig. 6), suggesting that 5B8 does not modulate peripheral adaptive immune responses. These results suggest that systemic delivery of 5B8 in vivo is well tolerated and that fibrin immunotherapy suppresses innate immune activation, oxidative stress, demyelination, and axonal damage in EAE.

Fibrin immunotherapy protects AD mice.

Neurodegeneration driven by the innate immune system has emerged as a key pathogenic mechanism in AD[29]. We therefore tested whether blocking fibrin/CD11b interactions protects against amyloid-related neurodegeneration. In 5XFAD mice, in which transgenes encoding familial AD-mutant forms of human amyloid precursor protein and presenilin 1 are expressed in neurons, fibrin was detected in the brain as early as 3 months of age; at 5 months, fibrin accumulation was abundant at sites of amyloid deposition, which were surrounded by $CD11b^+$ microglia (Fig. 6a, Supplementary Fig. 7a). In 5XFAD mice, fibrin deposits were detected in the vicinity of dystrophic neurites (Fig. 6b), a key feature of neurodegeneration in AD[30]. Systemically administered 5B8 spatially correlated with fibrin-rich areas surrounding amyloid plaques in 5XFAD mice (Fig. 6c, Supplementary Fig. 7b), demonstrating brain penetration and target engagement.

To determine whether blocking fibrin/CD11b interactions protects against amyloid-related neurodegeneration, we treated 5XFAD mice with 5B8 for 2 months, starting at 3.5 months of age (1.5 months after appearance of amyloid plaques and microglial activation) (Fig. 7a). 5B8 reduced reduced loss of cholinergic neurons and microglia activation around plaques in 5XFAD mice (Fig. 7b,c) without significantly affecting amyloid plaques or the number of $Mac2^+$ macrophages around plaques (Supplementary Fig. 8a,b). Whole-genome microarray and GO analysis of cortical gene expression in 5XFAD mice showed that 5B8 suppressed five key pathways: complement pathway, antigen presentation, cytokine response, lysozyme, and ROS (Fig. 7d). Overall, these findings suggest that blocking fibrin/CD11b signaling suppresses amyloid-induced neurodegeneration and reduces the expression of genes that promote inflammation and oxidative stress.

Fibrin immunotherapy suppresses *TYROBP* network genes.

Gene network analysis has broadened our understanding of AD pathogenesis by revealing immune gene networks as likely causal contributors to AD pathology[31]. Targeting these networks could culminate in the development of novel therapeutics. To identify gene networks that might be regulated by 5B8, we interrogated our transcriptomic data using biological network analysis. First, we performed genetic network modeling of genes downregulated by 5B8. We found a highly connected hub of co-expressed genes primarily within the complement pathway, including *TYROBP* (*DAP12*), *C4b*, and *C1q* (Fig. 8a). The 5B8-downregulated cluster of co-expressed genes shows a striking overlap with gene networks implicated in the pathogenesis of human AD, including those encoding the *TYROBP*-related microglial module[31]. Indeed, *TYROBP*, encoding a co-receptor for CD11b and the human AD-associated receptor *Trem2*, was one of the top 5B8-downregulated genes (Fig. 7d, Fig. 8a). Overlay of gene expression data obtained in 5B8-treated 5XFAD mice with neuroinflammatory gene networks from human AD brains showed a reduction of human AD-related inflammatory networks by 5B8. By overlaying our data on a mouse version of the human AD *TYROBP* module[31], we found that 5B8 downregulated 65% of the *Tyrobp*-related network at various levels of significance, including *Tyrobp* at the nexus of the network (Fig. 8b). Several components of the TYROBP signaling pathway were also downregulated (Supplementary Fig. 8c). This bioinformatic approach allowed us to gain insights into the mechanisms of action of 5B8 treatment, as we identified downregulation of co-expressed genes primarily within the complement pathway that were relevant to AD pathogenesis. Integrated gene network analysis could be a useful tool to better understand the mechanism of action of new drugs and assess their efficacy in suppressing inflammatory gene networks relevant to human disease. Thus, fibrin inhibition by 5B8 may suppress pathogenic activation of innate immune pathways that mediate amyloid-related neurodegeneration.

Discussion

Our study revealed a previously unknown neurodegenerative pathway in which fibrin activates NADPH oxidase in innate immune cells to promote ROS production and neurotoxicity. By developing an antibody-based approach to selectively target a key inflammatory fibrin domain, we showed here that fibrin-targeting immunotherapy can be

selective and efficacious in suppressing neuroinflammation and neurodegeneration. Consequently, preventing fibrin from engaging this mechanism may lead to the development of therapeutic strategies for neurodegenerative diseases with neurovascular dysfunction. This discovery may have implications beyond the CNS, since fibrin deposition is a common thread in inflammatory pathologies, such as rheumatoid arthritis, colitis, and Duchenne muscular dystrophy (reviewed in[11,12]). Fibrin/CD11b signaling induces chemokine release and macrophage recruitment[16] and increased NADPH oxidase activation culminating in ROS release and oxidative stress (this study). Therefore, inhibitors of fibrin/CD11b interaction, such as 5B8, have the potential to affect both inflammatory processes and oxidative stress. Inhibiting fibrin formation with anticoagulants can cause adverse effects by increasing bleeding risk[32]. Epitope-selective targeting of fibrin may overcome this challenge by selective suppression of its damaging functions without adverse anticoagulant effects. Overall, fibrin immunotherapy could represent a selective multi-indication therapy to suppress fibrin-induced chronic inflammation by inhibiting release of proinflammatory factors and oxidative stress at sites of increased vascular permeability in neurological and other inflammatory diseases.

Our study revealed a novel function of fibrin/CD11b signaling as an activator of NADPH oxidase-dependent ROS production. CD11b integrin-dependent respiratory bursts require DAP12 receptor signaling[33,] . CD11b and DAP12 are co-expressed in microglia and act synergistically to promote the production of superoxide ions and induce neuronal death[33]. Intriguingly, DAP12 was a major pathway downregulated by fibrin immunotherapy in the 5XFAD mouse brain. Fibrin—via activation of CD11b/CD18 signaling—might increase DAP12 expression and potentiate CD11b/DAP12-dependent oxidative damage by promoting the phosphorylation and assembly of the NADPH oxidase complex[34,35] and activating kinase pathways[13]. In addition to fibrin, several other immune-mediated mechanisms can activate NADPH oxidase, such as Aβ binding to CD36 scavenger receptor, or activation of CR3 or TLR4 signaling by α-synuclein or LPS[25]. Aβ-induced activation of NADPH oxidase in innate immune cells contributes to neurovascular dysfunction, neurodegeneration, and cognitive decline in AD mice[5,36]. Fibrin and Aβ may have an additive effect on NADPH oxidase activation via CD11b/CD18 and CD36, respectively. Genome-wide association studies, converged linkage analysis, and gene expression data have pointed to immune regulation of AD pathology. These studies, in combination with limited success of clinical trials targeting amyloid, have led to a reassessment of AD pathogenesis and the need for developing new treatments against different targets[37]. Vascular and amyloid pathologies are independent and additive predictors of cognitive decline in the elderly[38,39], suggesting that they may need to be targeted independently for maximal therapeutic benefit. Fibrin immunotherapy did not reduce Aβ deposition after 2 months of administration, suggesting that the neuroprotective effects of inhibiting fibrin/CD11b interactions occur in the presence of Aβ. Future studies will determine whether fibrin/CD11b signaling and 5B8 also affect cognitive performance in AD mice.

Fibrin immunotherapy represents a novel approach to selectively suppress pathogenic innate immune responses with potential clinical implications. In MS, anti-inflammatory medications have little effect in the progressive phase of disease, which is mediated by innate immune mechanisms[3,8]. Other modulators of innate immunity, such as complement,

CR3, TNF, NF-κB, PI3K, and TLR4, are ubiquitously expressed in the brain and the periphery and have reported roles in regulating physiological CNS functions. In contrast, fibrin is not present in the normal brain, but is abundantly deposited in the CNS after BBB disruption[11]. 5B8 is selective for inhibiting innate immune activation by fibrin-CR3 interactions and does not affect activation of macrophages by other ligands, such as LPS, suggesting that innate immune activation by other ligand/receptor interactions can proceed normally. Phagocytic pathways in innate immune cells are required for debris clearance and remyelination[40]. Fibrin-primed macrophages inhibit the differentiation of oligodendrocyte precursor cells[41], which are susceptible to oxidative stress[42]. Fibrin immunotherapy could suppress fibrin-induced chronic inflammation and potentially promote repair by inhibiting oxidative stress and release of proinflammatory factors. Microglia and macrophages are functionally distinct populations with diverse functions in neurodegenerative diseases[43–46]. Future studies using CyToF and large transcriptomic profiling in microglia and macrophages will be required to determine the potential differential effects of fibrin on innate immune populations. The fibrin $\gamma_{377–395}$ inflammatory epitope has been validated genetically in inflammatory models in the brain and periphery with findings replicated in numerous laboratories (reviewed in[11,12]). It is possible that pharmacologic targeting of fibrin-CR3 interactions could represent a selective treatment to add to the toolbox of anti-innate immune therapies that may be particularly efficacious for suppressing neuroinflammation at sites of BBB leakage and vascular damage with fibrin deposition.

The available genetic and pharmacologic tools used to study the $\gamma_{377–395}$ epitope (fibrinogen gamma chain $Fgg^{390–396A}$ mutant mice, $\gamma_{377–395}$ peptide, 5B8 antibody in this study) have primarily revealed pathogenic functions for the $\gamma_{377–395}$ epitope in inflammation. Fibrinogen alpha chain-deficient ($Fga^{-/-}$) and $Fgg^{390–396A}$ mice[13,47,48], mice treated with either 5B8 (this study) or $\gamma_{377–395}$ peptide[13], or anticoagulants[13,26,41] are not immunocompromised and can be housed in conventional animal facilities without opportunistic infections. In humans, congenital afibrinogenemia, a genetic disorder characterized by complete absence of fibrinogen, is associated with excessive bleeding but no increase in opportunistic infections[49]. Fibrin inhibits repair as persistent fibrin deposition inhibits wound healing[50], while fibrinogen depletion increases remyelination[41,51]. These studies do not exclude the possibility that the fibrinogen $\gamma_{377–395}$ epitope may have physiological functions that have not yet become apparent using the genetic and pharmacologic tools available. Collectively, prior genetic studies on the $\gamma_{377–395}$ epitope and our findings support that fibrin is inducing, in a ligand-selective manner, a specific gene signature in immune cells that produces primarily pathogenic functions. Consequently, targeting fibrin-induced activation of innate immunity has the potential to suppress proinflammatory and neurotoxic pathways without significant interference with protective functions of the innate immune system. Future immunotoxicology studies will also be required to fully test potential immune dysfunction in the context of fibrin immunotherapy.

Fibrinogen is a coagulation factor essential for blood clotting. Studies in $Fgg^{390–396A}$ mice have shown that the $\gamma_{377–395}$ epitope is not required for fibrin polymerization, platelet aggregation, and does not increase bleeding risk[48]. $Fgg^{390–396A}$ mice have normal fibrinogen concentrations, fibrin polymerization, platelet aggregation, normal thrombus formation in $FeCl_3$-injured carotid arteries, pregnancy and birth rates. Furthermore, they do

not develop spontaneous hemorrhagic events and tolerate major surgical procedures (e.g., abdominal surgeries), without inordinate bleeding[48]. In contrast to *Fgg*$^{390-396A}$ mice, *Fga*$^{-/-}$ mice that lack fibrinogen exhibit broad hemostatic abnormalities secondary to the lack of clotting function and failure of fibrinogen-supported platelet aggregation, and uniformly cannot sustain pregnancies due to hemostatic requirements at the placenta-maternal interface[47], a phenotype also observed in mice lacking fXIIIA[52]. Consistent with experimental findings in *Fgg*$^{390-396A}$ mice, the fibrin $\gamma_{377-395}$ peptide does not inhibit normal clotting time in vivo or fibrin polymerization *in vitro*[13]. Our study shows that 5B8 does not affect normal clotting time in vivo, fibrin polymerization in *vitro,* or aPTT in human plasma. Similar to the *Fgg*$^{390-396A}$ mice, mice treated with 5B8 even for prolonged periods up to ~2 months did not develop any spontaneous bleeding. The 5B8 $\gamma_{377-395}$ epitope does not overlap with the $\gamma_{398-406}$ residues known to be enzymatically cross-linked by transglutaminase fXIII[53]. Nevertheless, comparative studies of fXIII-mediated crosslinking *in vitro* and in vivo will be of interest in future studies of 5B8. This is could be of particular interest in light of studies of *Fgg*$^{390-396A}$ mice in a model of venous thrombosis[54]. Here, *Fgg*$^{390-396A}$ mice were shown to maintain fXIII-mediated γ chain cross-linking but at a reduced rate, and this resulted in smaller venous thrombi. Overall, studies in *Fgg*$^{390-396A}$ mice[48], data obtained with the fibrin $\gamma_{377-395}$ peptide[13] and in this study suggest that the $\gamma_{377-395}$ epitope and 5B8 do not interfere with fibrin clotting and presents limited risk of spontaneous hemorrhagic events. Future toxicology studies will be required to determine whether 5B8 may interfere with other features of hemostasis and thrombosis.

Together, data from human pathology, genetic and pharmacologic studies in mice, transcriptomic and signal transduction studies establish fibrin as a dual inflammatory and oxidative stress signal in the CNS and suggest that fibrin immunotherapy could prevent neurodegeneration and other complications in conditions associated with fibrin deposits at sites of BBB disruption. Fibrin immunotherapy may hold promise as a new therapeutic strategy for neurological and inflammatory disorders with vascular damage.

Methods

Methods, including statements of data availability and any associated accession codes and references, are available at <insert link here>

Animals.

SJL/J, C57BL/6, *Cx3cr1*$^{GFP/+}$ [55], *Thy1*-YFP (Tg(Thy1-YFP)HJrs)[56], 5XFAD (B6SJL-Tg (APPSwFlLon,PSEN1*M146L*L286V) 6799 Vas/Mmjax)[57], and *p47*$^{phox-/-}$[58] mice were purchased from The Jackson Laboratory and Sprague-Dawley rat P0 litters from Charles River Laboratories. 5XFAD were crossed with *Thy1*-YFP to generate 5XFAD:*Thy1*-YFP mice. *Ccr2*$^{RFP/RFP}$ on a C57BL/6 background provided by I. F. Charo (Gladstone Institutes), and bred to generate *Cx3cr1*$^{GFP/+}$*Ccr2*$^{RFP/+}$ mice[59]. Mice were housed in groups of five under standard vivarium conditions and a 12 h light/dark cycle. All animal protocols were approved by the Committee of Animal Research at the University of California, San Francisco, and in accord with the National Institutes of Health guidelines.

Mouse mAb production.

Synthesis of human fibrinogen $\gamma_{190–202}$ and $\gamma_{377–395}$ peptides and mouse monoclonal antibody production was performed by A&G Pharmaceuticals. Screening of 480 hybridomas was performed by ELISA against peptides or the carrier protein. Positive clones were expanded and retested to confirm peptide epitope reactivity to either $\gamma_{190–202}$ or $\gamma_{377–395}$. Target candidates were identified as outlined in Supplementary Fig. 1a. The structural map of the γC-domain of fibrinogen was generated using the PyMOL Molecular Graphics System, Version 1.6 Schrödinger, LLC with PDB ID 1FIC .

Peptide Binding assays.

Human $\gamma_{377–395}$ peptide (Genscript) in carbonate buffer (0.1 M $NaHCO_3$ and 0.15 M NaCl) was coated onto MaxiSorp ELISA plates (Thermo Fisher Scientific) overnight at 4 °C. Wells were incubated with blocking buffer (3% bovine serum albumin (BSA) and 0.1% NP-40 in PBS) for 2 h at 25 ˚C, washed with PBS 0.05% Tween-20. Antibodies 5B8, 4F1, 4E11, 1E3 were diluted in blocking buffer and added to the wells for 2 h at 25 ˚C followed by secondary polyclonal goat anti-mouse IgG/HRP (#P0447, DAKO) in blocking buffer for 2 h at 25 ˚C and developed by TMB substrate (Sigma-Aldrich) with 450_{nm} absorbance measured with an Envision Microplate reader (Perkin Elmer). For competition ELISA, the 5B8 antibody was diluted to 2 nM in blocking buffer and preincubated with increasing concentrations of human or mouse $\gamma_{377–395}$ and $\gamma_{190–202}$ peptides for 3 h at 25 ˚C. Competition of 5B8 to $\gamma_{377–395}$ or $\gamma_{190–202}$ was assessed by incubating on plates coated with human $\gamma_{377–395}$ peptide.

Fibrin/Fibrinogen binding.

Human plasminogen-free fibrinogen (#341578, EMD Millipore) was IgG depleted using Pierce albumin/IgG removal kit (Thermo Fisher Scientific). 25 μg/ml IgG-depleted human plasminogen-free fibrinogen in 20 mM HEPES pH 7.4 buffer was treated with 0.3 U/ml bovine thrombin (Sigma-Aldrich) and 7 mM $CaCl_2$ in MaxiSorp ELISA plates (Thermo Fisher Scientific) for 1.5 h at 37 °C. Formed fibrin was dried onto the wells at 37 °C overnight. 25 μg/ml IgG-depleted human fibrinogen was coated onto the wells at 37 °C for 2.5 h. Plates were washed with binding buffer (10 mM HEPES, pH 7.4 150 mM NaCl, 3 mM EDTA, and 0.05% Tween-20) and incubated with blocking buffer (binding buffer containing 3% BSA) for 1 h at 25 ˚C. Monoclonal antibodies in blocking buffer were incubated for 1 h at 25 ˚C. Following washing with binding buffer, polyclonal goat anti-mouse IgG/HRP (#P0447, DAKO) in blocking buffer was added for 1 h at 25 ˚C and signal was developed by Lumi-Phos HRP (Lumigen) measured with an Envision Microplate reader. Experiments of antibody binding to peptides, fibrin, and fibrinogen performed at the Gladstone Institutes were independently reproduced at the UCSF Small Molecule Discovery Center and at Lundbeck, US with similar results.

CD11b I-domain production.

pET15-His-TEV-CD11b was constructed by cloning the CD11b I-domain (residues Q130-S326) into a pET15b-derived plasmid at the NdeI and XhoI sites, preceded by an N-terminal 6xHis tag and followed by a TEV protease cleavage site (pET15-His-TEV-CD11b), then

transformed into Rosetta2(DE3) cells. Protein was expressed and purified as described[60], with the exception that cells were lysed using a pressure driven microfluidizer and His-containing proteins were trapped using TALON cobalt affinity resin. Protein purity was assessed to be > 90% by LC/MS and gel electrophoresis.

CD11b I-domain ELISA.

96-well ELISA plates (Greiner) were coated with 25 μg/ml fibrin or fibrinogen and incubated in blocking buffer as indicated for binding assays for 1 h prior to addition of 50 μl per well of biotinylated CD11b I-domain in PBS with 0.5% BSA and 0.05% Tween-20 for 2 h at 37 °C, followed by incubation with 1 μg/ml HRP-coupled Streptavidin (BD Pharmingen, 1:1000) for 1 h at 25 ˚C and developed by incubation with TMB/E substrate (Chemicon-Millipore) and absorbance measured at 450_{nm} with a Synergy H4 plate reader (BioTek). For 5B8 competition ELISA, after incubation in blocking buffer, 5B8 antibody was diluted at 2-fold concentrations from 0.02 μM to 10 μM and incubated for 2 h at 37 °C, followed by an incubation of 6.88 μM CD11b I-domain for 2 h at 25 ˚C.

Cell Culture.

Primary microglia and BMDMs were isolated, cultured, and treated with fibrin or LPS as previously described[16]. PBMCs (AllCells) (2×10^6 cells/mL) were plated in RPMI-1640 media supplemented with 10% heat-inactivated FBS, 1% penicillin-streptomycin, and 50 ng/ml human M-CSF (#300–25, Peprotech) in tissue-culture treated dishes (Corning). After 24 h, non-adherent cells were removed, and adherent cells were cultivated for 7–8 additional days at 37 °C in 5% CO_2.

Morphometry.

Primary microglia were stimulated with fibrin for 48 has described[16]. Microglia were fixed with 4% PFA, permeabilized with 0.1% Triton X-100 and immunostained with FITC-labeled Isolectin B4 (1:300; Sigma-Aldrich) and/or CellMask™ Red Stain (Thermo Scientific). Blocking involved pre-incubation with 80 μg/ml antibodies or mouse IgG2b (clone MPC-11, BioXCell BE0086 distributed by the UCSF Monoclonal Antibody Core, endotoxin concentrations < 0.002 EU/μg) or IgG2b (eBiosciences endotoxin level < 0.01 EU/μg) for 2 h at 37 °C before plating of cells for a final concentration of antibodies at 40 μg/ml. Manual Analysis: Images were collected using an Axioplan 2 Zeiss microscope with an Axiocam HRc camera and analyzed using ImageJ. 250 cells per condition were counted for each experiment. Activated microglia were classified based on a surface area > 2,000 μm^2. Automated Image Acquisition and Analysis: Images of microglia cells were acquired with the GEHC IN-Cell Analyzer 2000™, using a 10× lens and excitation/emission filter pairs of $350_{nm}/455_{nm}$ (CellMask™ Red Stain) and $579_{nm}/624_{nm}$ (Hoechst dye). Images were analyzed with the GEHC IN-Cell Developer Toolbox version 1.9. The Hoechst-stained nuclei were segmented using a “nuclear” segmentation type, with a set minimum target area of 30 μm^2 and set sensitivity of 75%. To minimize artifacts, segmentation with less than 120 intensity units or area greater than 1000 μm^2 were excluded. The CellMask™ Red-stained whole microglia cells were segmented using an “intensity” segmentation type, with a set threshold between 200 – 4095 intensity units. The borders of adjacent contacting cells were resolved using the “clump breaking” segmentation post-processing, which utilizes discrete

nuclei as seeds. For segmented by size cells > 800 μm^2 were classified as activated microglia. Only cells containing a nucleus within the cell body area were accepted. All segmented nuclei and cells were then recorded as individual counts.

Fibrin polymerization assay.

Human fibrinogen was diluted to 0.15 mg/ml in 20 mM HEPES (pH 7.4) containing 0.15 M NaCl and 5 mM ε-amino caproic acid and combined with 0.3 U/ml thrombin (Sigma-Aldrich), and 10 mM $CaCl_2$. Antibodies (50 μg/ml) or GPRP peptide (Bachem) were incubated with fibrinogen for 2 h at 37 °C before mixing with $CaCl_2$/thrombin. Absorbance at 350_{nm} over intervals of 60 s was measured using a SpectraMax M5 microplate reader (Molecular Devices) with SoftMax Pro 5.2 software (Phoenix Technologies Ltd.).

Plasma clotting time and aPTT assay.

Plasma-clotting times were measured as described[13] by combining equal volumes of citrated plasma and 2 U/ml bovine thrombin (Enzyme Research Laboratories) and 40 mM $CaCl_2$ at 37 °C. aPTT assay was performed in pooled normal human plasma (Innovative Research) using 50 μg/ml 5B8 or IgG2b or 0.5 mM GPRP peptide (Bachem). Plasma was incubated with 5B8 or IgG2b at 37 °C for 2 h. Clotting was initiated by aPTT-XL (Ellagic acid activator) and 0.02 M $CaCl_2$ (Thermo Fisher Scientific) and monitored at 405_{nm} in a SpectraMax M5 microplate reader.

Real time qPCR, multi-plex qPCR and microarray analysis.

RNA isolation, real-time PCR, and microarray analysis were performed as described[16]. Primers are listed in Supplementary Table 3. Microarray data from GEO GSE71084 were used to select ROS genes with significant log_2 expression to generate heat maps for primary microglia and BMDMs. For multiplex qPCR, primary microglia were plated in 96-well black μ-clear-bottom microtiter plates (Greiner Bio-One) in DMEM, 10 % FBS, 1 % penicillin/streptomycin and allowed to adhere for 24 h prior to being treated for 4 h with 1 μM fibrin D-dimer (HyTest) as described[12]. 20 μg/ml 5B8 or IgG2b were pre-incubated with fibrin D-dimer in DMEM for 3 h at 37 ºC before cell treatment. Gene expression was assessed using the RT2 Profiler PCR Array (Rat Inflammatory & Autoimmunity; Qiagen), and only differentially expressed genes (fold > 2, $P < 0.05$) were reported as the mean fold change. Gene expression antibody inhibition experiments performed at the Gladstone Institutes were independently reproduced at Lundbeck, US with similar results.

Oxidant detection with DHE.

BMDMs or PBMCs were incubated in RPMI containing 5 μM DHE (Invitrogen) for 30 min. 100,000 cells/well were plated on 96-well black μ-clear-bottom microtiter plates (Greiner Bio-One) precoated with 25 μg/ml fibrin. 20 μg/ml 5B8 or IgG2b (UCSF Monoclonal Antibody Core clone LTF-2) were added in fibrin-coated wells 2 h before plating cells. BMDMs were incubated with 300 μM apocynin (Calbiochem) for 1 h or 5 μg of anti-CD11b (M1/70, eBioscience) for 30 min before plating. Cells were incubated on fibrin for 24–48 h, fixed with 4% PFA for 10 min, and DHE fluorescence was detected at $518_{nm}/605_{nm}$ using

SpectraMax M5 microplate reader. Cells were quantified by DAPI counterstaining. In mice, in vivo DHE administration and detection was performed as described[15].

NADPH oxidase activity.

BMDMs were plated on 25 μg/ml fibrin-coated 6-well plates (Greiner Bio-One). 20 μg/ml 5B8 or IgG2b were added to the fibrin plates 2 h before plating cells. NADPH oxidase activity was assayed by the lucigenin-enhanced chemiluminescence method[61]. Cells were collected by a cell scraper and homogenized in ice-cold Krebs buffer pH 7.4 (119 mM NaCl, 2.5 mM KCl, 1mM NaH_2PO_4, 1.3 mM $MgCl_2$, 2.5 mM $CaCl_2$, 11 mM glucose, and 20 mM HEPES, pH 7.4). The cell homogenate was centrifuged at 1000g, and the pellet was resuspended with luminescence buffer (Krebs buffer containing 10 μM lucigenin, Cayman Chemicals), before adding 100 μM NADPH substrate (Sigma-Aldrich). Luminescence was detected by an EnSpire microplate reader.

Immunoblots.

BMDMs cultured on 25 μg/ml fibrin-coated plates were lysed in RIPA lysis buffer (EMD Millipore) with protease/phosphatase inhibitor cocktail (EMD Millipore). Protein extracts (20 μg) were separated by electrophoresis on NuPAGE 4–12% Bis-Tris Gel (Life Technologies) and transferred onto nitrocellulose. Blots were blocked in 5% milk in TBST and incubated with gp91phox (1:1000; clone EPR6991, Abcam), Phospho-p40phox (1:1000; Thr154, Cell Signaling Technology), and GAPDH (1:5000; clone 14C10, Cell Signaling Technology) using horseradish peroxidase-conjugated secondary antibody (1:5000; Cell Signaling Technology #7074S) and enhanced chemiluminescence (ECL) kit (GE Healthcare) for detection. Densitometry analysis was performed using ImageJ.

Cortical neuron-macrophage co-culture.

Cortices from P1 rats were finely minced and digested for 30 min at 37 °C in DPBS (Gibco) containing papain (Worthington Biochemicals) and DNase (Sigma-Aldrich). Papain was inhibited by the addition of ovomucoid (Worthington Biochemicals). Neurons were plated at a density of 60,000 cells/cm^2 on poly-D-lysine pre-coated 8-well Permanox chamber slides (Sigma-Aldrich) in Neurobasal/B27 medium (Invitrogen) and cultured for 10 days. Rat BMDMs were cultured in RPMI-1640 with 10% heat-inactivated FBS (Invitrogen), 1% penicillin-streptomycin (Corning), and 10 ng/ml rat M-CSF (#400–28, Peprotec). BMDMs were plated on 25 μg/ml fibrin-coated plates with 20 μg/ml 5B8 or IgG2b for 24 h and were lifted with PBS-EDTA as described[16] and added to cortical neuron cultures for two days, fixed with 4% PFA and immunostained with anti-MAP-2 (1:1000; clone AP20, EMD Millipore) and thresholded images were quantified with the NeurphologyJ plug-in in ImageJ. 2.5×10^{10} GC/ml of AAV1.hSyn.TurboRFP (University of Pennsylvania Vector Core) was used to transduce primary cortical neurons for 8 d prior to the addition of fibrin-stimulated BMDMs for 12 h. RFP images were thresholded and the neurite fragments were analyzed using the ImageJ plugin ‘Analyze Particles’. Quantification was performed by an observer blinded to the experimental treatments.

Pharmacokinetics.

C57BL/6 mice were injected with 400 μg 5B8 i.p. Blood samples were collected by micro-accusampler and centrifuged at 2500 rpm for 15 min. Plasma was stored at −80 °C until analysis. Plasma was diluted 1:1000 in blocking buffer (3% BSA and 0.1% NP-40 in PBS). 5B8 was diluted in blocking buffer to create a concentration curve. Plasma and 5B8 were added to wells coated with human $\gamma_{377–395}$ peptide and incubated for 2 h at 25 ˚C. After washing, polyclonal goat anti-mouse IgG-HRP (#P0447, DAKO) in blocking buffer was added for 2 h at 25 ˚C and the assay was developed with TMB Liquid substrate (Sigma-Aldrich) with absorbance measured using an Envision Microplate reader.

EAE.

EAE was induced in 8–9-week-old female SJL/J, C57BL/6, or *Cx3cr1*$^{GFP/+}$*Ccr2*$^{RFP/+}$ mice by subcutaneous immunization with 100 μg $PLP_{139–151}$ (HSLGKWLGHPDKF; Auspep Pty Ltd) or 50 μg $MOG_{35–55}$ (MEVGWYRSPFSRVVHLYRDGK; Auspep Pty Ltd) in complete Freund's adjuvant (Sigma-Aldrich) supplemented with 400 μg of heat-inactivated mycobacterium tuberculosis H37Ra (Difco Laboratories). Two days after immunization, mice were injected i.p. with 200 ng (C57BL/6) or 75 ng (SJL/J) pertussis toxin (Sigma-Aldrich). For adoptive transfer, donor SJL/J mice were immunized as described above, and on day 10, cells from draining lymph nodes and spleen were isolated. Lymphocytes were re-stimulated with 20 μg/ml $PLP_{139–151}$ peptide and 10 ng/ml of IL-12 (eBioscience) for 4 d, and 3×10^7 cells were transferred into healthy SJL/J recipients. Frequency of donor $CD4^+$ T cells producing IFNγ by FACS was assessed before transfer. For prophylactic treatment, mice were each given 800 μg of either 5B8 or isotype-control IgG2b every two days from day 0. For therapeutic treatment, antibodies were injected every two days starting at the peak of the initial paralytic episode. Mice were observed daily and clinical scores were assessed by observers blinded to treatments as follows: 0, no symptoms; 1, loss of tail tone; 2, ataxia; 3, hindlimb paralysis; 4, hindlimb and forelimb paralysis; 5, moribund.

Histology and immunohistochemistry.

For histological analysis, spinal cords and brains were processed as described[13,62]. Antibodies used were: mouse anti-neurofilament H non-phosphorylated (1:100; BioLegend clone SMI-32), rabbit anti-Iba-1 (1:1000; Wako #019–19741), and mouse anti-myelin basic protein (1:100; BioLegend clone SMI-99) and Alexa Fluor 488 or 594 (1:500; Jackson ImmunoResearch) for detection. Immunohistochemistry for anti-MBP was performed with the Mouse on Mouse (M.O.M.) kit (Vector Labs). *Ccr2*$^{RFP/+}$*Cx3cr1*$^{GFP/+}$ mice were perfused with 4% PFA and spinal cord segments were frozen in OCT, then cut into 10-μm sections and stained with DAPI for 5 min. DHE labeling was performed as described [15]. For analysis of 5XFAD mice, mice were perfused with 4% PFA and brains were postfixed in 4% PFA overnight at 4 °C, except for CD11b staining, which was postfixed for 4 h. Immunohistochemistry in coronal brain sections (30 μm) were performed using antibodies against ChAT (1:1000, EMD Millipore #AB144P), CD11b (1:150; eBioscience clone M1/70), Iba-1 (1:1000; Wako), Mac-2 (1:1000; Cedarlane clone M3/38), fibrinogen (1:1000; J. L. Degen, Cincinnati Children's Hospital Medical Center), and human Aβ (1:500; IBL-America #18584). Amyloid plaques were labeled with methoxy-XO4 (fluorescent probe for

Aβ, Tocris) as described[63]. Images were acquired with an Axioplan II epifluorescence microscope (Zeiss) equipped with dry Plan-Neofluar objectives (10 × 0.3 NA, 20 × 0.5 NA, or 40 × 0.75 NA) or all-in-one BZ-X700 fluorescence microscope (Keyence) or a Fluoview FV1000 (Olympus) confocal microscope and FluoView Software v3.1b. Excitation lasers were set to 405, 488, and 543_{nm} and Olympus 20 × 1.00 NA, Olympus 25 × 1.05 NA, or an Olympus 40 × 0.8 NA water immersion lens with 1.0 μm *z*-step and Kalman filtering using line mode of 2 were used. Iba1, Aβ, Mac2+ quantification was averaged from 9 field of views of high Aβ plaque density throughout the cortex. Images were quantified using ImageJ by observers blinded to the experimental conditions.

Flow cytometry.

Primary mouse splenocytes were isolated from 5B8- and IgG2b-treated mice 10 days after immunization with $PLP_{139–151}$. Cell suspensions were stained with combinations of antibodies: CD45 (BioLegend clone 30-F11), CD3 (BioLegend clone 17A2), CD4 (BioLegend clone GK1.5), CD11b (BioLegend clone M1/70), B220 (BD Bioscience clone RA3–6B2), Ly6G (eBioscience clone RB6–8C5), and CD11c (BioLegend clone N418). For cytokine analysis, cells were incubated for 4 h with Cell Activation Cocktail (BioLegend) and surface stained for CD3, CD4, and CD8 (BioLegend clone 53–6.7). Cells were then fixed with Cytofix/Cytoperm solution (BD Biosciences), and intracellular cytokine staining was performed with anti-IFN-γ (BioLegend clone XMG1.2) and anti-IL-17-FITC (BioLegend clone TC11–18H10.1). All antibodies were used at 1:300. Flow cytometry was performed on an LSR II (BD Biosciences). Data were analyzed using FlowJo (Tree Star).

Stereotactic fibrinogen injection and drug treatment.

Stereotactic injection of fibrinogen into the corpus callosum of *Cx3cr1*$^{GFP/+}$ or C57BL/6 mice and analysis were performed as described[15,16]. 5B8, or 5B8-F(ab) fragment, or isotype-control IgG2b (clone MPC-11, eBioscience) was injected (10 μg at 0.2 μl/min) into the cerebral ventricle (AP, −2.0 mm; ML, 0 mm, DV, −2.0 mm) with a 10-μl syringe attached to a 33-gauge needle 30 min before fibrinogen injection.

5B8 penetration in the CNS and target engagement.

Mice were injected i.p. with 800 μg/mouse of biotinylated 5B8 every 2 days (3 total doses). Mice were perfused with saline, and spinal cord or brain were processed for fresh frozen sections as described. Sections were fixed with 4% PFA for 10 min and biotinylated 5B8 was detected using Cy3-conjugated streptavidin (1:100; Invitrogen) for 30 min at 25 ˚C. Sections were incubated for 1h with fibrinogen antibody (1:2000), followed by FITC donkey anti-rabbit (1:500; Jackson ImmunoResearch) for 30 min at 25 ˚C. For amyloid plaque staining, sections were counterstained with Methoxy-X04 (Tocris; 4% vol of 10 mg/ml).

Two-photon in vivo imaging.

Thy1-YFP and *Thy1*-YFP:5XFAD mice were injected with Alexa594-conjugated fibrinogen (Invitrogen) intravenously daily for 3 days as described[15]. Mice were also injected i.p. with Methoxy-X04 24 h prior to imaging. Methoxy-X04 was solubilized with DMSO:propylene glycol:PBS pH 7.5 (ratio 2:9:9) at 5 mg/ml. On day of imaging, a small craniotomy was

made and a custom-made metal plate affixed to a stage to stabilize the skull. Alexa594-fibrinogen solution was injected retro-orbitally prior to imaging. The anesthetized animal was placed on a heated pad under an Ultima-IV multiphoton microscope (Prairie) equipped with MaiTai DeepSee-eHP lasers (Spectra Physics). The excitation wavelength was 820_{nm} to simultaneously visualize fibrinogen, methoxy-X04 and YFP dendrites. Imaging was performed from 20 to 150 μm below the dura, using a Nikon 40 × 0.8 NA -immersion lenses with a 1.0 μm *z*-step. *z*-stacks of images were projected along the *z*-axis to recreate two-dimensional representations of the 3D structures within the imaged volumes. Images were adjusted for brightness, contrast and background noise with ImageJ. Spectral unmixing plugin in ImageJ was used to separate overlapping signals.

Network analyses.

The TYROBP network and the Microglia Pathogen Phagocytosis Pathway were translated from human-specific, static figures to mouse-specific data models using WikiPathways[73] and HomoloGene, The coexpression network was constructed by extracting the dominant cluster of downregulated genes of interest (selected from those with $\log_2$ fold change of −0.02 or less and raw *P*-value < −0.05) based on coexpression interaction data provided by GeneMANIA[74]. Subsequent network visualization, layout, data overlays and subnetwork extraction were performed in Cytoscape[75].

Statistical analyses.

Data are presented as mean ± s.e.m. Statistical calculations were performed with GraphPad Prism (Version 6.03). Sample sizes were based on previous experiments and not predetermined by statistical methods. Statistical significance was determined with non-parametric two-sided Mann-Whitney test, Kruskal-Wallis test, Welch's two-sample t-test, one-way or two-way analysis of variance followed by Bonferroni or Tukey's post-test (multiple comparisons). Linear models were fitted for each gene using the Bioconductor 'limma' package in R[64]. Moderated *t*-statistics, fold change and the associated *P* values were calculated for each gene. Mice were randomly assigned to experimental groups for EAE and 5XFAD experiments. Scoring of EAE mice was performed in a blinded fashion. All animals survived until the end of the study and all data points were included in analysis. All histopathological analysis and quantification was performed blinded.

To compare EAE clinical scores, the linear mixed effects models were performed using the R statistical package. Means of maximum clinical scores were compared using a two-sample t-test as implemented in R using the Welch's *t*-test and the Wilcoxon rank sum test. *P*-values were corrected for multiple testing using the Holm procedure. The statistical significance of the changes in the mean clinical score for each day of the experiment was estimated using permutation tests. The corresponding p-values were estimated using 1000 permutations in all prophylactic antibody treatment and 10000 permutations for therapeutic antibody treatment. In each permutation, mice were randomly permuted. To compare the first day of onset, the log-rank test was used as implemented by the *survdiff* function in the *survival* package in R.

Supplementary Material

Refer to Web version on PubMed Central for supplementary material.

Acknowledgements

We thank J.L. Degen for expert advice and critical reading of the manuscript and S. Pintchovski, I. Kadiu, J. Palop, and J. Egebjerg for insightful discussions. We thank B. Cabriga, R. Meza Acevedo, L. Ta, and A. Williams for expert technical assistance, G. Maki for graphics, G. Howard and K. Claiborne for editorial. The Gladstone Center for In Vivo Imaging Research was supported in part by grants from H. Lundbeck A/S, the S.D. Bechtel, Jr. Foundation, and the Conrad N. Hilton Foundation 17348 to K.A. The microscopy studies were carried out in part at facilities adapted for this project at the National Center for Microscopy and Imaging Research, which is supported by grant P41 GM10341 awarded to M.H.E. Gladstone Institutes was supported by NIH/NCRR grant RR18928. The Mouse Pathology Core of the UCSF Helen Diller Family Comprehensive Cancer Center was supported by CA082103. J.K.R, D.D., and A.S.M. were supported by National Multiple Sclerosis Society (NMSS) Postdoctoral Fellowships; J.K.R. and D.D by Race to Erase MS Young Investigator Awards and American Heart Association (AHA) Scientist Development Grants; V.A.R. by postdoctoral fellowships from AHA and NIH/NINDS F32 NS096920; A.S.M. by NIAID T32AI733429 and NMSS FG-1708–28925, K.K.H. by NSF predoctoral fellowship DGE-0648991/1144247; M.A.P. by a NIH/NICHD K12-HD072222; L.M. by a gift from the Dolby Family; S.S.Z. by NIH R01 NS092835; R21 NS108159, NMSS RG1701–26628, RG 5179A10/2, the Weill Institute, and the Maisin Foundation; R.A.S by NIH R01 NS081149. This work was supported by grants from NMSS RG3782, H. Lundbeck A/S, the Conrad N. Hilton Foundation 17348, a gift from the Levine Family, and NIH/NINDS R01 NS052189, R21 NS082976, and R35 NS097976 to K.A.

H. Lundbeck A/S sponsored research in K.A.'s laboratory at the Gladstone Institutes. K.A. is a co-founder and scientific advisor of MedaRed, Inc. K.A. is an inventor on University of California issued patents US7807645, US8569242, US8877195, and US8980836 covering fibrin antibodies. K.A. and J.K.R are co-inventors on Gladstone Institutes issued patent US9669112 covering fibrin in vivo models and Gladstone Institutes pending US20160320370 patent application covering in vitro fibrin assays. K.A., A.M.F., M.R.A., and K.K.A. are co-inventors on the Gladstone Institutes and University of California pending US20170003280 patent application covering assays for inhibition of microglia activation. Their interests are managed by the Gladstone Institutes in accordance with its conflict of interest policy. J.B.S., R.B.N., S.B.P, L.O.P, V.M., S.H.Z. were Lundbeck employees during the time the work was performed.

References

1. Rivest S Regulation of innate immune responses in the brain. Nat Rev Immunol 9, 429–439 (2009). [PubMed: 19461673]
2. Ransohoff RM & Brown MA Innate immunity in the central nervous system. J Clin Invest 122, 1164–1171 (2012). [PubMed: 22466658]
3. Lassmann H, van Horssen J & Mahad D Progressive multiple sclerosis: pathology and pathogenesis. Nat Rev Neurol 8, 647–656 (2012). [PubMed: 23007702]
4. Schuh C et al. Oxidative tissue injury in multiple sclerosis is only partly reflected in experimental disease models. Acta Neuropathol 128, 247–266 (2014). [PubMed: 24622774]
5. Heppner FL, Ransohoff RM & Becher B Immune attack: the role of inflammation in Alzheimer disease. Nat Rev Neurosci 16, 358–372 (2015). [PubMed: 25991443]
6. Lassmann H Mechanisms of neurodegeneration shared between multiple sclerosis and Alzheimer's disease. J Neural Transm 118, 747–752 (2011). [PubMed: 21373761]
7. Nikic I et al. A reversible form of axon damage in experimental autoimmune encephalomyelitis and multiple sclerosis. Nat Med 17, 495–499 (2011). [PubMed: 21441916]
8. Chitnis T & Weiner HL CNS inflammation and neurodegeneration. J Clin Invest 127, 3577–3587 (2017). [PubMed: 28872464]
9. Frischer JM et al. The relation between inflammation and neurodegeneration in multiple sclerosis brains. Brain 132, 1175–1189 (2009). [PubMed: 19339255]
10. Zhao Z, Nelson AR, Betsholtz C & Zlokovic BV Establishment and Dysfunction of the Blood-Brain Barrier. Cell 163, 1064–1078 (2015). [PubMed: 26590417]
11. Petersen MA, Ryu JK & Akassoglou K Fibrinogen in neurological diseases: mechanisms, imaging and therapeutics. Nat Rev Neurosci 19, 283–301 (2018). [PubMed: 29618808]

12. Davalos D & Akassoglou K Fibrinogen as a key regulator of inflammation in disease. Semin Immunopathol 34, 43–62 (2012). [PubMed: 22037947]
13. Adams RA et al. The fibrin-derived gamma377–395 peptide inhibits microglia activation and suppresses relapsing paralysis in central nervous system autoimmune disease. J Exp Med 204, 571–582 (2007). [PubMed: 17339406]
14. Ugarova TP et al. Sequence gamma 377–395(P2), but not gamma 190–202(P1), is the binding site for the alpha MI-domain of integrin alpha M beta 2 in the gamma C-domain of fibrinogen. Biochemistry 42, 9365–9373 (2003). [PubMed: 12899623]
15. Davalos D et al. Fibrinogen-induced perivascular microglial clustering is required for the development of axonal damage in neuroinflammation. Nat Commun 3, 1227 (2012). [PubMed: 23187627]
16. Ryu JK et al. Blood coagulation protein fibrinogen promotes autoimmunity and demyelination via chemokine release and antigen presentation. Nat Commun 6, 8164 (2015). [PubMed: 26353940]
17. Yates RL et al. Fibrin(ogen) and neurodegeneration in the progressive multiple sclerosis cortex. Ann Neurol 82, 259–270 (2017). [PubMed: 28719020]
18. Marik C, Felts PA, Bauer J, Lassmann H & Smith KJ Lesion genesis in a subset of patients with multiple sclerosis: a role for innate immunity? Brain 130, 2800–2815 (2007). [PubMed: 17956913]
19. Lee NJ et al. Spatiotemporal distribution of fibrinogen in marmoset and human inflammatory demyelination. Brain 141, 1637–1649 (2018). [PubMed: 29688408]
20. Strickland S Blood will out: vascular contributions to Alzheimer's disease. J Clin Invest 128, 556–563 (2018). [PubMed: 29388925]
21. Nathan C & Cunningham-Bussel A Beyond oxidative stress: an immunologist's guide to reactive oxygen species. Nat Rev Immunol 13, 349–361 (2013). [PubMed: 23618831]
22. Fischer MT et al. NADPH oxidase expression in active multiple sclerosis lesions in relation to oxidative tissue damage and mitochondrial injury. Brain 135, 886–899 (2012). [PubMed: 22366799]
23. Shimohama S et al. Activation of NADPH oxidase in Alzheimer's disease brains. Biochem Biophys Res Commun 273, 5–9 (2000). [PubMed: 10873554]
24. Ma MW et al. NADPH oxidase in brain injury and neurodegenerative disorders. Mol Neurodegener 12, 7 (2017). [PubMed: 28095923]
25. Haslund-Vinding J, McBean G, Jaquet V & Vilhardt F NADPH oxidases in oxidant production by microglia: activating receptors, pharmacology and association with disease. Br J Pharmacol 174, 1733–1749 (2017). [PubMed: 26750203]
26. Han MH et al. Proteomic analysis of active multiple sclerosis lesions reveals therapeutic targets. Nature 451, 1076–1081 (2008). [PubMed: 18278032]
27. Davalos D et al. Early detection of thrombin activity in neuroinflammatory disease. Ann Neurol 75, 303–308 (2014). [PubMed: 24740641]
28. Haider L et al. Oxidative damage in multiple sclerosis lesions. Brain 134, 1914–1924 (2011). [PubMed: 21653539]
29. Heneka MT et al. Neuroinflammation in Alzheimer's disease. Lancet Neurol 14, 388–405 (2015). [PubMed: 25792098]
30. DeKosky ST & Scheff SW Synapse loss in frontal cortex biopsies in Alzheimer's disease: correlation with cognitive severity. Ann Neurol 27, 457–464 (1990). [PubMed: 2360787]
31. Zhang B et al. Integrated systems approach identifies genetic nodes and networks in late-onset Alzheimer's disease. Cell 153, 707–720 (2013). [PubMed: 23622250]
32. Shoeb M & Fang MC Assessing bleeding risk in patients taking anticoagulants. J Thromb Thrombolysis 35, 312–319 (2013). [PubMed: 23479259]
33. Mocsai A et al. Integrin signaling in neutrophils and macrophages uses adaptors containing immunoreceptor tyrosine-based activation motifs. Nat Immunol 7, 1326–1333 (2006). [PubMed: 17086186]
34. Bedard K & Krause KH The NOX family of ROS-generating NADPH oxidases: physiology and pathophysiology. Physiol Rev 87, 245–313 (2007). [PubMed: 17237347]

35. Turnbull IR & Colonna M Activating and inhibitory functions of DAP12. Nat Rev Immunol 7, 155–161 (2007). [PubMed: 17220916]
36. Park L et al. Scavenger receptor CD36 is essential for the cerebrovascular oxidative stress and neurovascular dysfunction induced by amyloid-beta. Proc Natl Acad Sci U S A 108, 5063–5068 (2011). [PubMed: 21383152]
37. Cummings J Lessons Learned from Alzheimer Disease: Clinical Trials with Negative Outcomes. Clin Transl Sci 11, 147–152 (2018). [PubMed: 28767185]
38. Vemuri P et al. Vascular and amyloid pathologies are independent predictors of cognitive decline in normal elderly. Brain 138, 761–771 (2015). [PubMed: 25595145]
39. Rabin JS et al. Interactive Associations of Vascular Risk and beta-Amyloid Burden With Cognitive Decline in Clinically Normal Elderly Individuals: Findings From the Harvard Aging Brain Study. JAMA Neurol (2018).
40. Miron VE et al. M2 microglia and macrophages drive oligodendrocyte differentiation during CNS remyelination. Nat Neurosci 16, 1211–1218 (2013). [PubMed: 23872599]
41. Petersen MA et al. Fibrinogen Activates BMP Signaling in Oligodendrocyte Progenitor Cells and Inhibits Remyelination after Vascular Damage. Neuron 96, 1003–1012 e1007 (2017). [PubMed: 29103804]
42. Oka A, Belliveau MJ, Rosenberg PA & Volpe JJ Vulnerability of oligodendroglia to glutamate: pharmacology, mechanisms, and prevention. J Neurosci 13, 1441–1453 (1993). [PubMed: 8096541]
43. Butovsky O et al. Identification of a unique TGF-beta-dependent molecular and functional signature in microglia. Nat Neurosci 17, 131–143 (2014). [PubMed: 24316888]
44. Ajami B et al. Single-cell mass cytometry reveals distinct populations of brain myeloid cells in mouse neuroinflammation and neurodegeneration models. Nat Neurosci 21, 541–551 (2018). [PubMed: 29507414]
45. Keren-Shaul H et al. A Unique Microglia Type Associated with Restricting Development of Alzheimer's Disease. Cell 169, 1276–1290 (2017). [PubMed: 28602351]
46. Mrdjen D et al. High-Dimensional Single-Cell Mapping of Central Nervous System Immune Cells Reveals Distinct Myeloid Subsets in Health, Aging, and Disease. Immunity 48, 380–395 (2018). [PubMed: 29426702]
47. Suh TT et al. Resolution of spontaneous bleeding events but failure of pregnancy in fibrinogen-deficient mice. Genes Dev 9, 2020–2033 (1995). [PubMed: 7649481]
48. Flick MJ et al. Leukocyte engagement of fibrin(ogen) via the integrin receptor alphaMbeta2/Mac-1 is critical for host inflammatory response in vivo. J Clin Invest 113, 1596–1606 (2004). [PubMed: 15173886]
49. Lak M, Keihani M, Elahi F, Peyvandi F & Mannucci PM Bleeding and thrombosis in 55 patients with inherited afibrinogenaemia. Br J Haematol 107, 204–206 (1999). [PubMed: 10520042]
50. Bugge TH et al. Loss of fibrinogen rescues mice from the pleiotropic effects of plasminogen deficiency. Cell 87, 709–719 (1996). [PubMed: 8929539]
51. Akassoglou K, Yu W-M, Akpinar P & Strickland S Fibrin inhibits peripheral nerve regeneration by arresting Schwann cell differentiation. Neuron 33, 861–875 (2002). [PubMed: 11906694]
52. Koseki-Kuno S, Yamakawa M, Dickneite G & Ichinose A Factor XIII A subunit-deficient mice developed severe uterine bleeding events and subsequent spontaneous miscarriages. Blood 102, 4410–4412 (2003). [PubMed: 12933578]
53. Chen R & Doolittle RF - cross-linking sites in human and bovine fibrin. Biochemistry 10, 4487–4491 (1971). [PubMed: 5168975]
54. Aleman MM et al. Factor XIII activity mediates red blood cell retention in venous thrombi. J Clin Invest 124, 3590–3600 (2014). [PubMed: 24983320]
55. Jung S et al. Analysis of fractalkine receptor CX(3)CR1 function by targeted deletion and green fluorescent protein reporter gene insertion. Mol Cell Biol 20, 4106–4114 (2000). [PubMed: 10805752]
56. Feng G et al. Imaging neuronal subsets in transgenic mice expressing multiple spectral variants of GFP. Neuron 28, 41–51 (2000). [PubMed: 11086982]

57. Oakley H et al. Intraneuronal beta-amyloid aggregates, neurodegeneration, and neuron loss in transgenic mice with five familial Alzheimer's disease mutations: potential factors in amyloid plaque formation. J Neurosci 26, 10129–10140 (2006). [PubMed: 17021169]

58. Jackson SH, Gallin JI & Holland SM The p47phox mouse knock-out model of chronic granulomatous disease. J Exp Med 182, 751–758 (1995). [PubMed: 7650482]

59. Saederup N et al. Selective chemokine receptor usage by central nervous system myeloid cells in CCR2-red fluorescent protein knock-in mice. PLoS One 5, e13693 (2010). [PubMed: 21060874]

60. Jensen MR et al. Structural Basis for Simvastatin Competitive Antagonism of Complement Receptor 3. J Biol Chem 291, 16963–16976 (2016). [PubMed: 27339893]

61. Abid MR, Spokes KC, Shih SC & Aird WC NADPH oxidase activity selectively modulates vascular endothelial growth factor signaling pathways. J Biol Chem 282, 35373–35385 (2007). [PubMed: 17908694]

62. Davalos D et al. Fibrinogen-induced perivascular microglial clustering is required for the development of axonal damage in neuroinflammation. Nat Commun 3, 1227 (2012). [PubMed: 23187627]

63. Klunk WE et al. Imaging Abeta plaques in living transgenic mice with multiphoton microscopy and methoxy-X04, a systemically administered Congo red derivative. J Neuropathol Exp Neurol 61, 797–805 (2002). [PubMed: 12230326]

64. Gentleman RC et al. Bioconductor: open software development for computational biology and bioinformatics. Genome Biol 5, R80 (2004). [PubMed: 15461798]

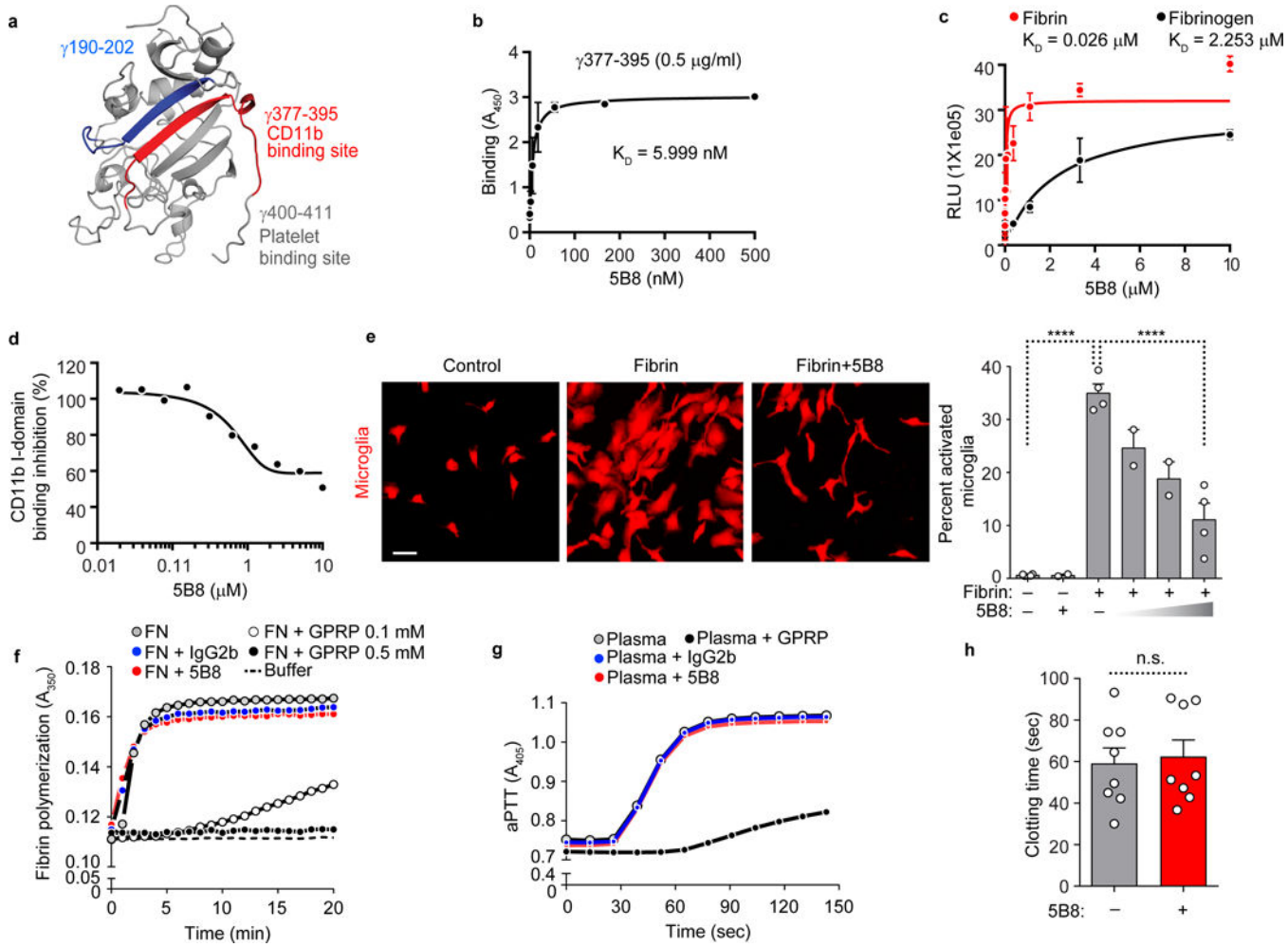

Fig. 1 | . Generation and characterization of monoclonal antibody 5B8 targeting the $\gamma_{377–395}$ fibrin epitope.

a, Structural map of cryptic epitope $\gamma_{377–395}$ in the γC-domain of fibrinogen. The $\gamma_{377–395}$ epitope (red) includes a core β-strand and portion of the fibrin γC-domain's C-terminal loop and binds to the CD11b I-domain. **b**, Binding affinity of 5B8 to $\gamma_{377–395}$ measured by ELISA. Data are mean ± s.e.m. of 4 independent experiments. **c**, Comparison of 5B8 binding to fibrin and fibrinogen by ELISA. Data are mean ± s.e.m. of 3 independent experiments. **d**, 5B8 competition with the CD11b I-domain for binding to fibrin by competitive ELISA. Data shown from one experiment. **e**, Microglia stimulated with fibrin in the presence of 5B8 (10, 20, and 40 μg/ml). Representative images are shown from unstimulated, and fibrin-treated microglia in the absence or presence of 40 μg/ml 5B8. Scale bar, 10 μm. Quantification of microglia activation (increased cell size) at 48 h after treatment is shown. Data are mean ± s.e.m. from 4 independent experiments (untreated, fibrin, fibrin + 40 μg/ml 5B8) analyzed with manual and automated quantification with similar results. ****$P < 0.0001$ by one-way analysis of variance (ANOVA) with Sidak's multiple comparisons test. **f**, *In vitro* fibrin polymerization was examined in the presence of fibrinogen (FN) alone or with 5B8, IgG2b, or GPRP. Data are representative of two independent experiments with similar results. **g**, aPTT assay was performed in human

plasma in the presence of 5B8, IgG2b, or GPRP. Data are representative of two independent experiments with similar results. **h**, In vivo clotting times of blood from 5B8-injected mice and uninjected controls. Data are mean ± s.e.m.; n = 8 mice per treatment. $P = 0.7768$ (two-tailed Mann-Whitney test); n.s., not significant.

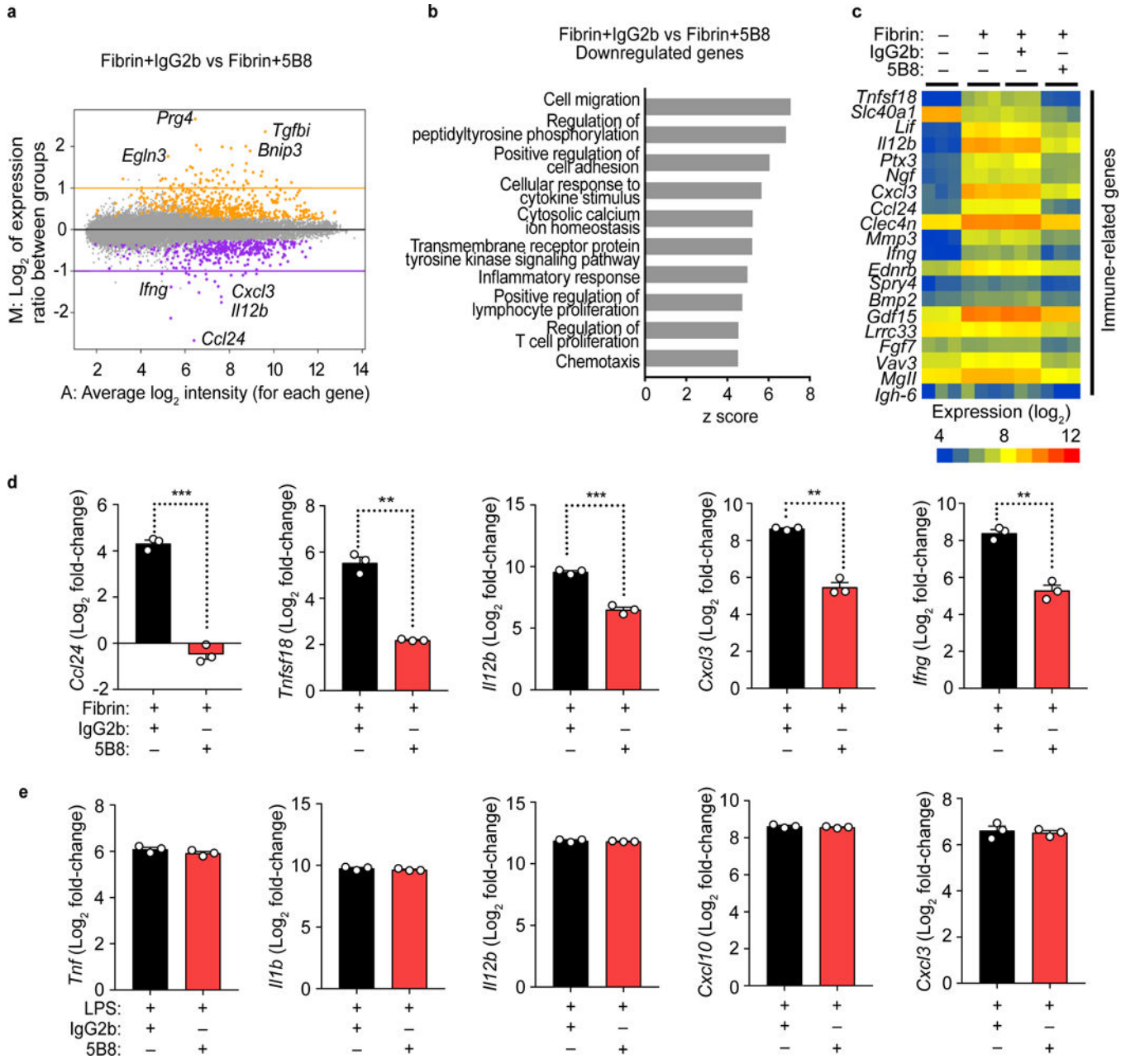

Fig. 2 | . Gene expression changes by 5B8 treatment of fibrin-stimulated BMDMs.

a, MA plot of whole-genome microarray analysis of 5B8- vs. IgG2b-treated BMDMs 6 h after fibrin stimulation. Colors indicate genes whose expression was significantly increased (orange) or decreased (purple) by 5B8; the remaining genes are in gray. Data are from 3 independent experiments. Linear models were fitted for each gene using the Bioconductor 'limma' package in R. Moderated t-statistics, fold change and the associated P values were calculated for each gene (two-tailed, raw $P < 0.001$). **b**, The top 10 biological processes relevant to 5B8-reduced innate/adaptive immune transcripts in BMDMs were identified by GO-Elite analysis (Z score >2.0, $P < 0.05$) **c**, Heat map of the top 20 transcripts that were significantly downregulated after 5B8 treatment of fibrin-stimulated BMDMs. Whole-

genome microarray data from 3 independent experiments. **d**, Relative expression of transcripts of proinflammatory genes *Ccl24*, *Tnfsf18*, *Il12b*, *Cxcl3*, and *Ifng* in fibrin-stimulated BMDMs treated with 5B8 or IgG2b, measured by qRT-PCR. Y-axis indicates $\log_2$ value of relative fold changes in qRT-PCR results. Data are mean ± s.e.m. from 3 independent experiments. *** $P = 0.0001$ (*Ccl24*), ** $P = 0.0052$ (*Tnfsf18*), *** $P = 0.0010$ (*Il12b*), ** $P = 0.0050$ (*Cxcl3*), and ** $P = 0.0015$ (*Ifng*) by unpaired two-tailed t-test with Welch's correction. **e**, 5B8 had no effect on LPS-induced gene expression in BMDMs analyzed by qRT-PCR. Y-axis indicates $\log_2$ value of relative fold changes in qRT-PCR results. Data are mean ± s.e.m. from 3 independent experiments. No significant difference by unpaired two-tailed *t*-test with Welch's correction.

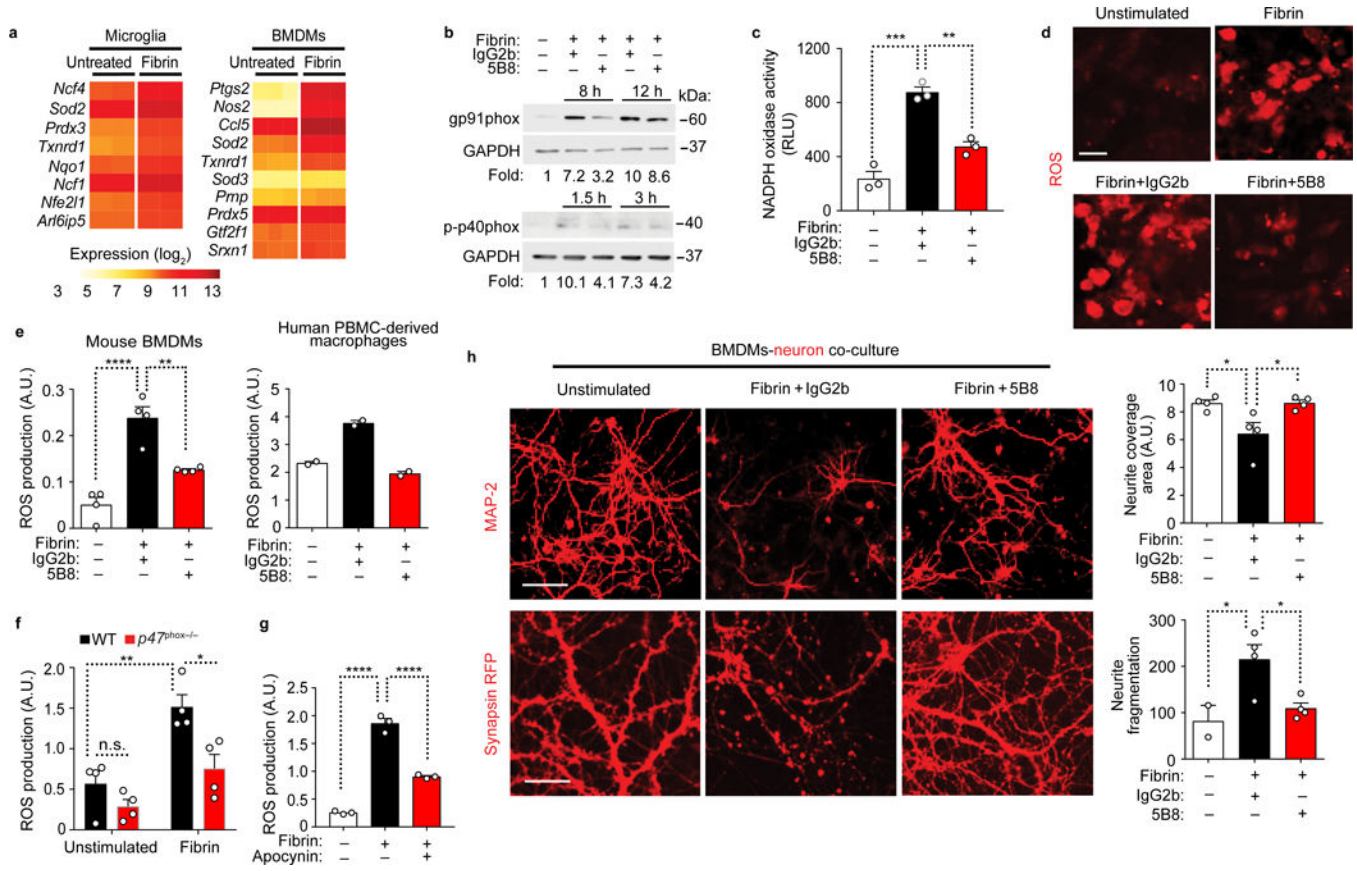

Fig. 3 | . 5B8 blocks fibrin-induced ROS production and axonal damage.

a, Heat map of significantly differentially expressed ROS-related genes in fibrin-induced microglia and BMDMs ($|\log_2$ fold change$| > 0.585$ and FDR < 0.05; two-tailed moderated *t*-test). **b**, Immunoblot for gp91phox and p-p40phox in BMDMs stimulated with fibrin as indicated in the presence of 5B8 or IgG2b. Representative cropped blot images from 3 independent experiments are shown. Full blots are included in Supplementary Fig. 9. **c**, NADPH oxidase activity in 12 h fibrin-stimulated BMDMs in the presence of 5B8 or IgG2b. Data are mean ± s.e.m. of 3 independent experiments. RLU, relative chemiluminescent light units. ** $P = 0.0015$ and *** $P = 0.0001$ by one-way ANOVA with Tukey's multiple comparisons test. **d**, ROS production by fibrin-stimulated BMDMs detected with dihydroethidium (DHE, red). Scale bar, 10 μm. Data are representative of three independent experiments with similar results. **e**, Quantification of ROS production by DHE in BMDMs (left) and human PBMC-derived macrophages (right) 48 h after fibrin stimulation in the presence of 5B8 or IgG2b. Data are mean ± s.e.m. of 4 (left graph) and 2 (right graph) independent experiments. A.U., arbitrary units. ** $P = 0.0033$, **** $P < 0.0001$ (mouse BMDMs) by one-way ANOVA with Bonferroni multiple comparisons test. **f**, ROS production 24 h after fibrin stimulation in BMDMs isolated from WT and *p47*$^{phox–/–}$ mice. Data are mean ± s.e.m. of n = 4 mice per group. A.U. * $P = 0.0204$, ** $P = 0.0040$ by two-way ANOVA with Sidak's multiple comparisons test. n.s., not significant. **g**, ROS production measured by DHE in murine BMDMs 24 h after fibrin stimulation in the presence of apocynin. Data are mean ± s.e.m. of 3 independent experiments. A.U.-- **** *P*

< 0.0001 by one-way ANOVA with Tukey's multiple comparisons test. **h**, MAP-2^+ (upper panel) and synapsin-RFP (lower panel) cortical neurons co-cultured with unstimulated or fibrin-stimulated BMDMs in the presence of 5B8 or IgG2b. Scale bars, 50 μm (top panels) and 30 μm (bottom panels). Quantification of MAP-2^+ neurites (top) and synapsin-RFP^+ neurites (bottom). Data are mean ± s.e.m. from 4 independent experiments * $P = 0.0385$ (unstimulated vs Fibrin+IgG2b, top), * $P = 0.0370$ (Fibrin+IgG2b vs Fibrin+5B8, top); * $P = 0.0168$ (Fibrin+IgG2b vs Fibrin+5B8, bottom) by one-way ANOVA with Bonferroni multiple comparisons test.

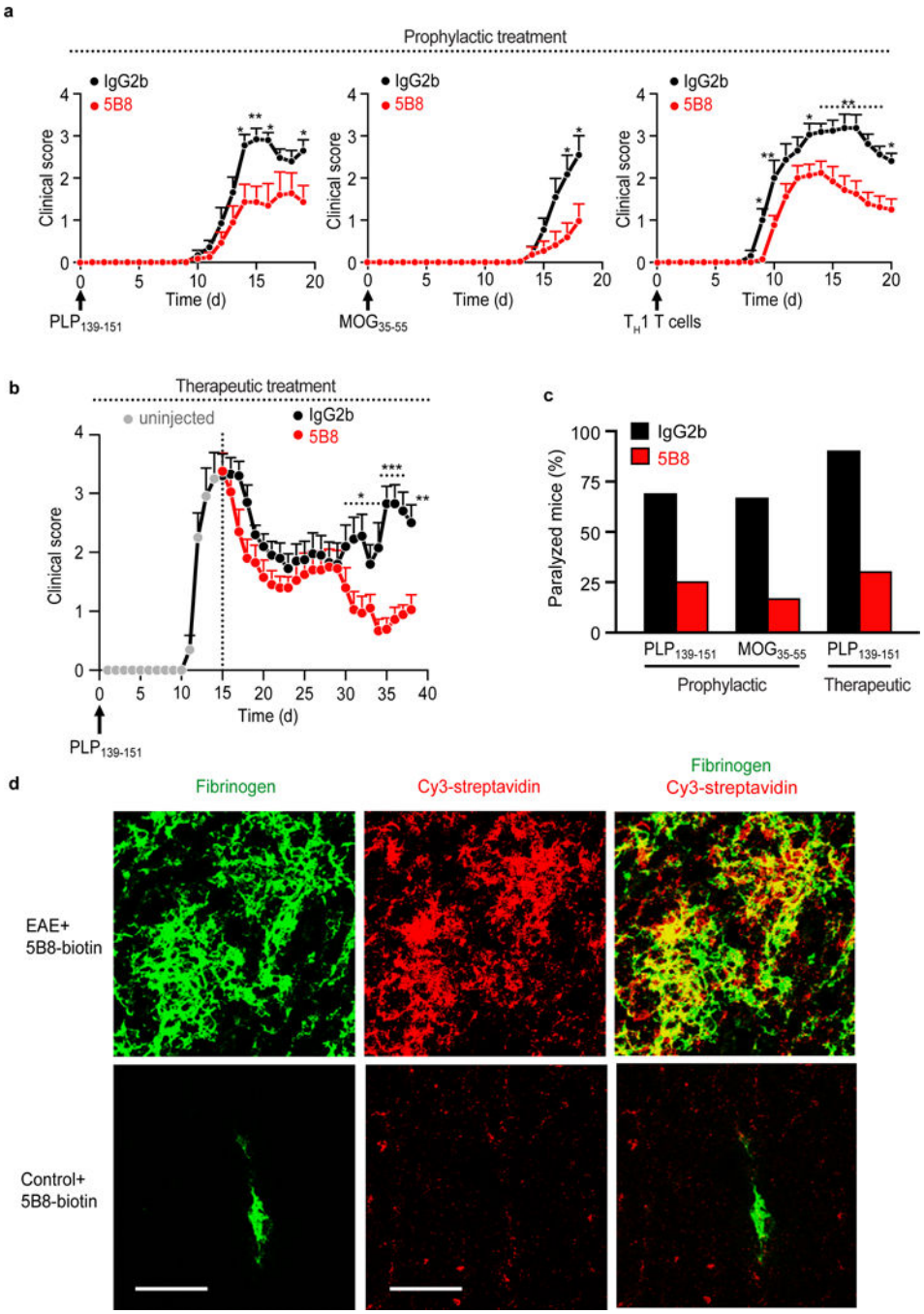

Fig. 4 | . 5B8 suppresses EAE and engages fibrin target.

a, Reduction of clinical signs after 5B8 administration in four EAE models. Prophylactic administration of 5B8 or IgG2b isotype control in $PLP_{139–151}$, $MOG_{35–55}$, and adoptive transfer T_H1 EAE (* $P < 0.05$, ** $P < 0.01$, linear mixed effects model with two-tailed permutation test). Mice were each given 800 μg of either 5B8 or isotype-control IgG2b every two days from day 0. Data are mean ± s.e.m. from $PLP_{139–151}$ (n = 16 IgG2b and n = 16 5B8), $MOG_{35–55}$ (n = 11 IgG2b and n = 12 5B8), and T_H1 EAE (n = 15 IgG2b and n = 24 5B8) **b**, Therapeutic administration of 5B8 or IgG2b isotype control in $PLP_{139–151}$ EAE

after peak of disease (* $P < 0.05$, ** $P < 0.01$, *** $P < 0.001$, linear mixed effects model with two-tailed permutation test). For therapeutic treatment, antibodies were injected every two days starting at the peak of the initial paralytic episode. Data are mean ± s.e.m. from $PLP_{139–151}$ EAE (n = 10 IgG2b and n = 10 5B8). **c**, Effect of 5B8 treatment on the percentage of paralyzed mice (defined as partial or complete hindlimb paralysis, score >2.5) in three EAE groups. **d**, Target engagement of i.p. injected biotinylated 5B8 in $MOG_{35–55}$ EAE mice and healthy non-immunized control mice. Confocal microscopy of spinal cord sections from $MOG_{35–55}$ EAE mice shows the spatial correlation (yellow) between biotinylated 5B8, detected with Cy3-streptavidin (red), and fibrin deposition, detected with a fibrin(ogen) antibody (green), in $MOG_{35–55}$ EAE mice. Representative images are shown from n = 3 mice per group. Scale bar, 200 μm.

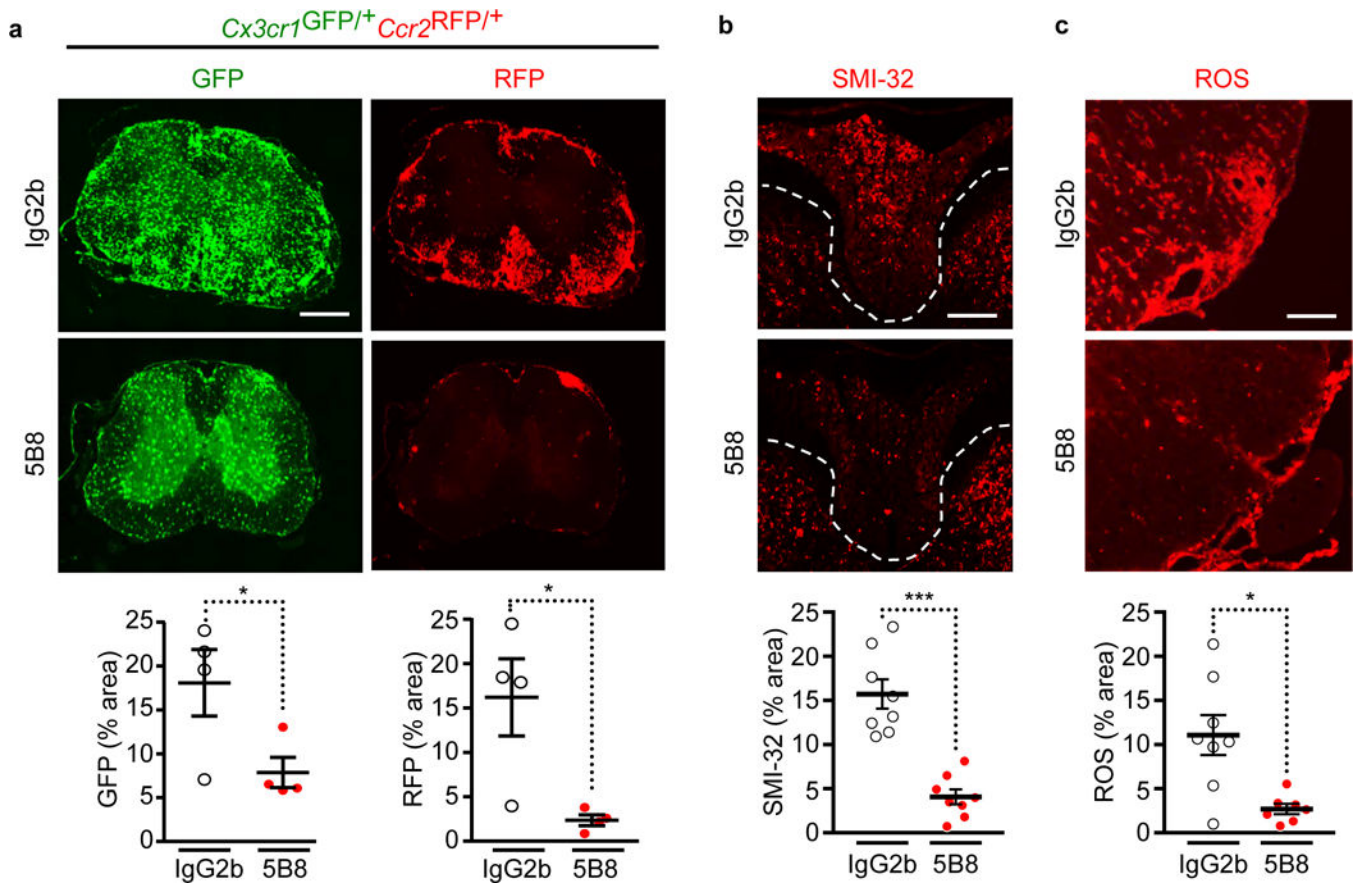

Fig. 5 | . 5B8 inhibits microglial activation, monocyte recruitment, and axonal damage in EAE.

a, Spinal cord images of 5B8- or IgG2b-treated $MOG_{35–55}$ EAE *Cx3cr1*$^{GFP/+}$*Ccr2*$^{RFP/+}$ mice. Scale bar, 500 μm. Quantification of $Cx3cr1^+$ microglia (GFP, green) and $Ccr2^+$ macrophages (RFP, red). Data are mean ± s.e.m.; n = 4 mice per treatment. * $P = 0.0495$ (GFP), * $P = 0.0286$ (RFP), by two-tailed Mann-Whitney test. **b**, SMI-32 immunoreactivity indicative of axonal damage in spinal cords of 5B8- or IgG2b-treated $PLP_{139–151}$ EAE mice. Scale bar, 200 μm. Dotted lines indicate spinal cord dorsal column white matter. Quantification of SMI-32 immunoreactivity. Data are mean ± s.e.m.; n = 8 mice per group. *** $P = 0.0002$, two-tailed Mann-Whitney test. **c**, ROS detection in the spinal cord with DHE of 5B8- or IgG2b-treated $PLP_{139–151}$ EAE mice. Scale bar, 100 μm. Quantification of DHE. Data are mean ± s.e.m.; n = 8 IgG2b and n = 7 5B8. * $P = 0.0140$ by two-tailed Mann-Whitney test.

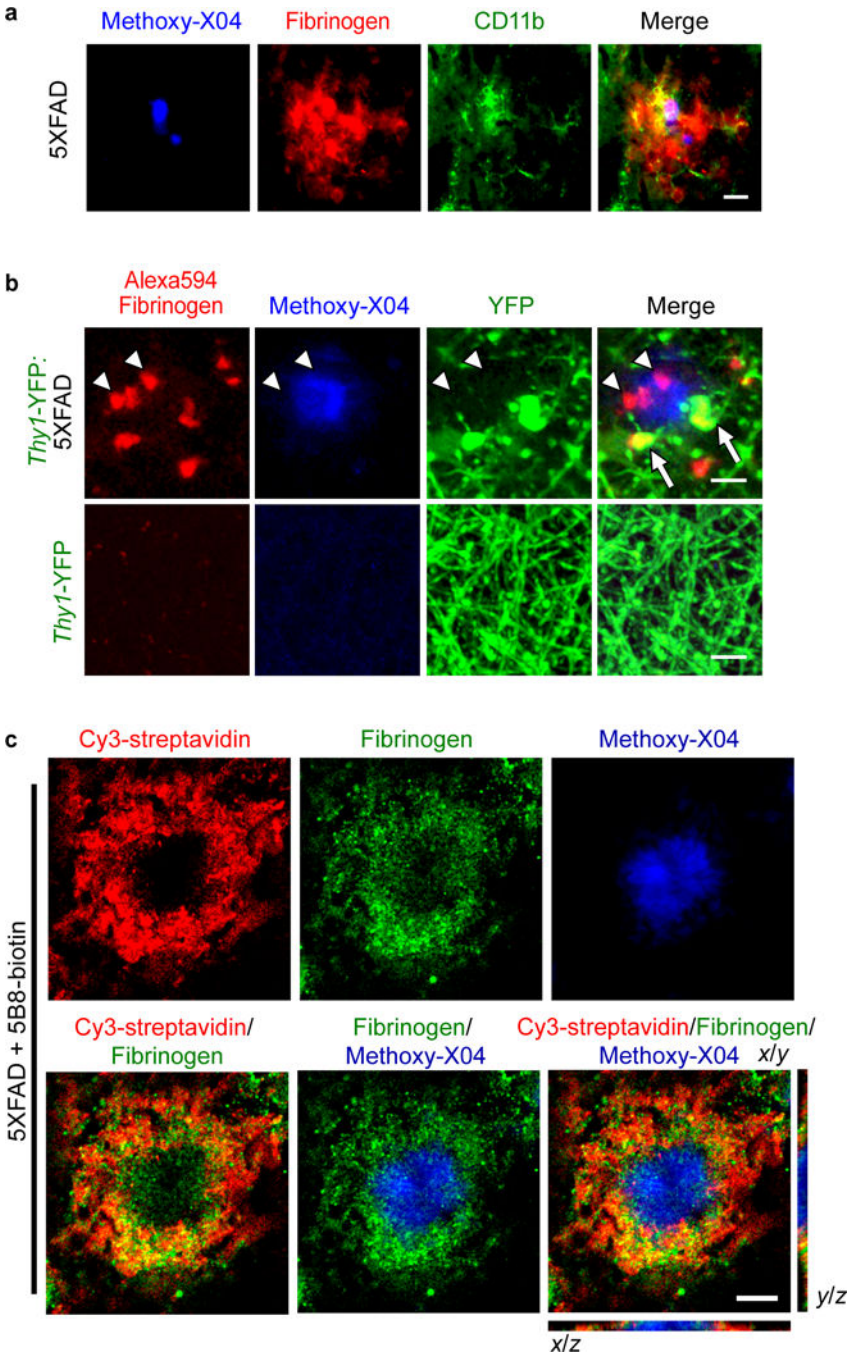

Fig. 6 | . In vivo imaging of fibrinogen leakage in 5XFAD mice.

a, Fluorescent Aβ probe methoxy-X04-positive amyloid plaque in a cortical section from a 3-month-old 5XFAD mouse co-labeled for fibrinogen (red) and CD11b (green). Scale bar: 20 μm. n = 4 mice. Representative images are shown. **b**, In vivo two-photon imaging of cortex from *Thy1*-YFP:5XFAD mice at 11 months of age shows Alexa594-conjugated fibrinogen (administered intravenously) (red), a methoxy-X04-positive Aβ plaque (blue), and dystrophic neurites (green, swollen green structures). Arrowheads indicate fibrinogen (red) surrounding a Aβ plaque (blue) at areas of neuritic loss. Arrows indicate fibrinogen

extravasation at areas of dystrophic neurites (yellow) in proximity to a plaque (blue). Scale bars: 10 μm. (n = 4 *Thy1*-YFP:5XFAD mice and n = 2 *Thy1*-YFP mice. Representative images are shown. **c**, 5B8 in vivo target engagement in the brain of 5XFAD mice. Brain sections of 5XFAD i.p.-injected with biotinylated 5B8 were stained with Cy3-streptavidin (red), anti-fibrinogen (green), and methoxy-X04-positive Aβ plaque (blue). Orthogonal views of the *y/z* and *x/z* planes show localization of fibrinogen and 5B8 antibody around amyloid plaques. Scale bar, 10 μm. n =3 mice Representative images are shown.

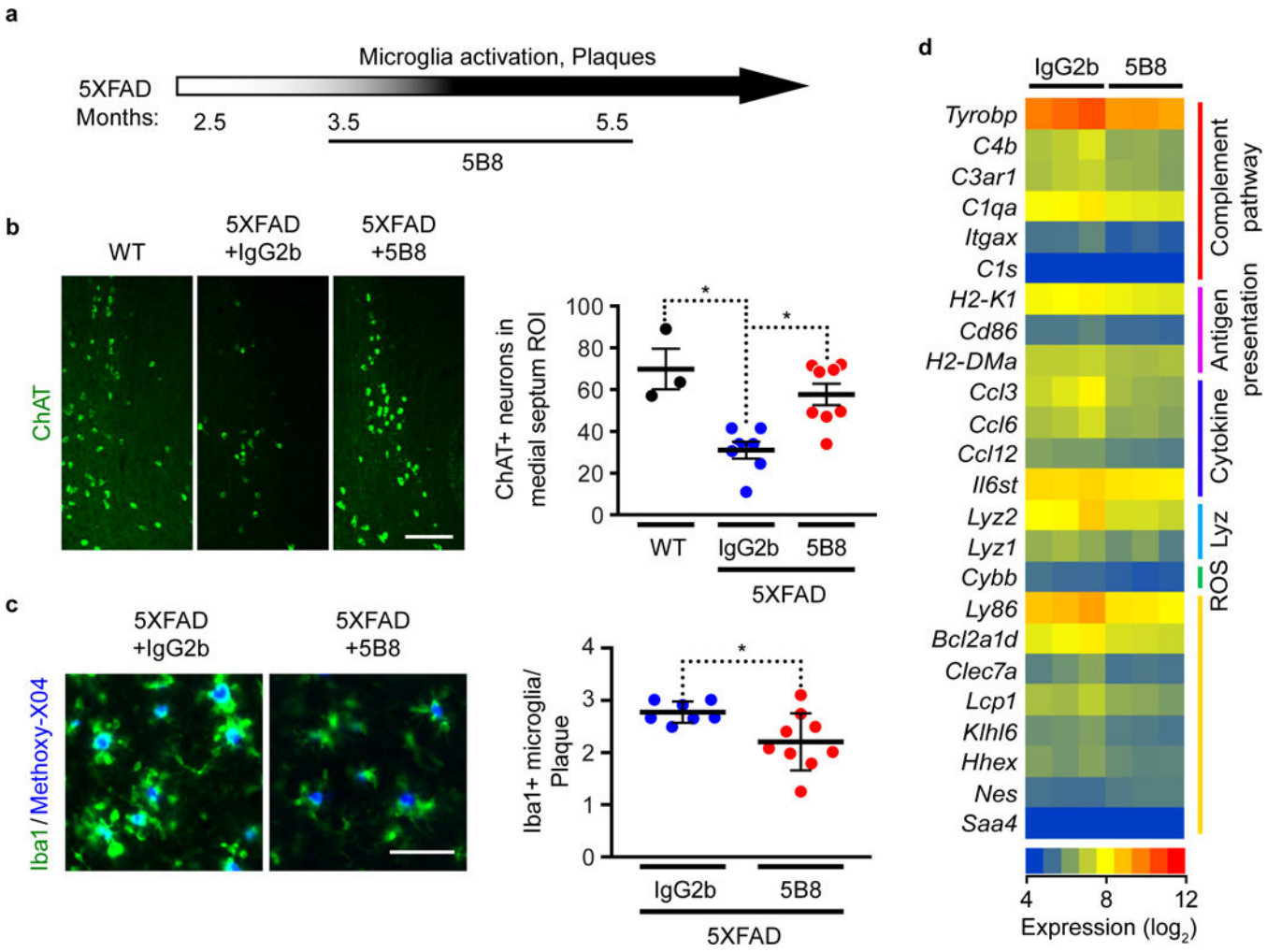

Fig. 7 | . 5B8 protects against neurodegeneration and inflammatory responses in 5XFAD mice.
a, Schematic representation of 5B8 administration after appearance of plaques and microglia activation in 5XFAD mice (800 μg i.p. every other day for 2 months starting at 3.5 months of age). **b**, ChAT-positive cholinergic neurons in the medial septum of non-transgenic littermate control (WT), 5XFAD mice treated with IgG2b or 5B8. Scale bars 80 μm. Quantification of ChAT+ neurons. Data are mean ± s.e.m.; $n = 3$ WT, $n = 7$ IgG2b-treated and $n = 8$ 5B8-treated 5XFAD mice. * $P = 0.0211$ (WT vs IgG2b), * $P = 0.0157$ (IgG2b vs 5B8) by Kruskal–Wallis with Dunn's multiple comparisons test. **c**, Iba-1$^+$ cells (green) around Methoxy-X04$^+$ plaques (blue) in the cortex of 5XFAD mice treated with IgG2b or 5B8. Quantification of plaque-associated Iba-1+ microglia. Scale bar: 50 μm. Data are mean ± s.e.m.; n = 7 IgG2b-treated and $n = 9$ 5B8-treated 5XFAD mice. * $P = 0.0337$ by two-tailed Mann-Whitney test. **d**, Affymetrix microarray gene expression analysis in the cortex of 5B8- or IgG2b-treated 5XFAD mice. Linear models were fitted for each gene using the Bioconductor 'limma' package in R. Moderated t-statistics, fold change and the associated P values were calculated for each gene (two-tailed, raw $P < 0.05$). Heatmap of select genes with differential expression patterns from GO terms were identified by GO-Elite analysis.

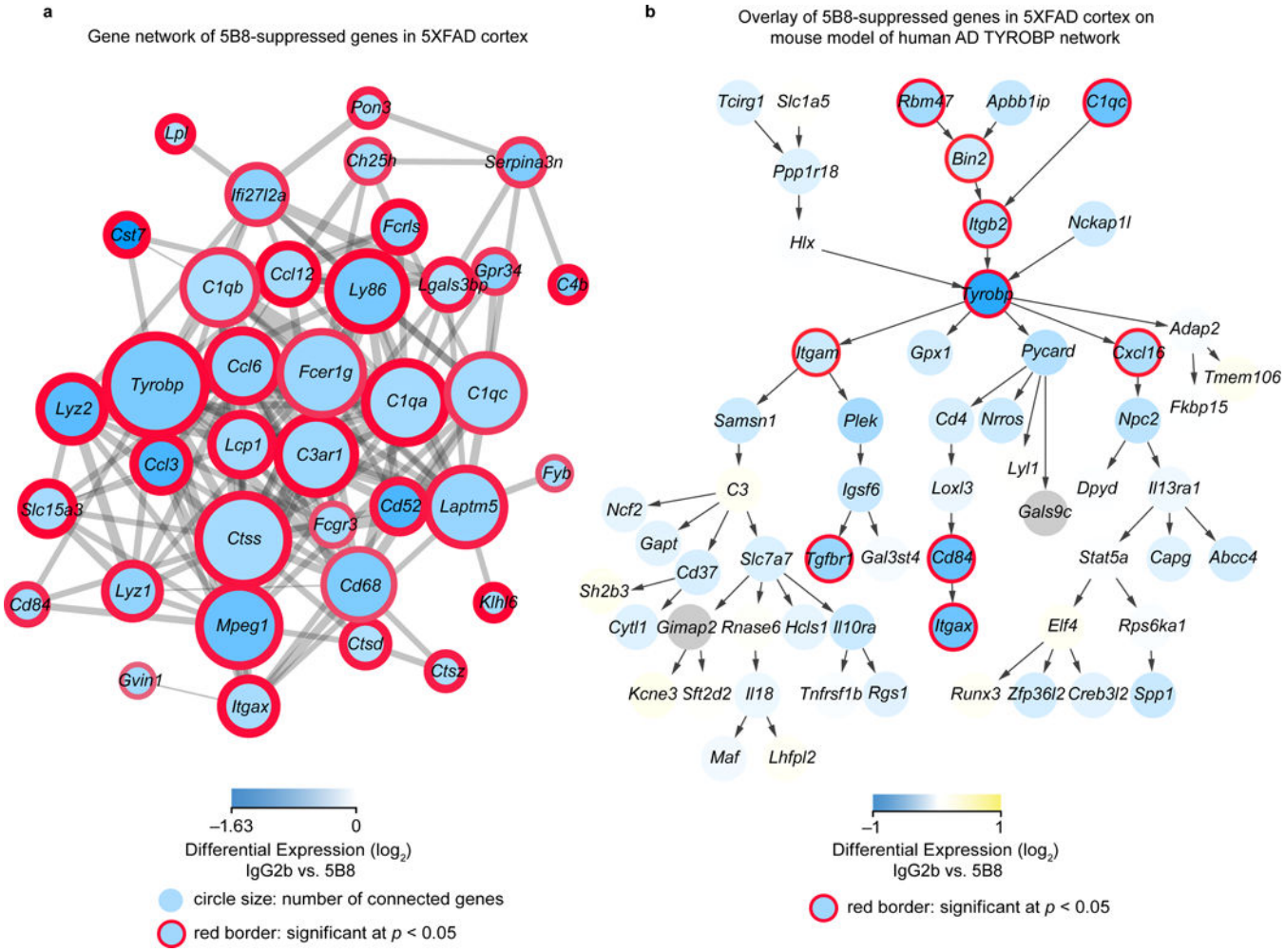

Fig. 8 | . 5B8 suppresses the complement/TYROBP microglial module in 5XFAD mice.

a, Co-expression analysis revealed 5B8-downregulated genes to be densely interconnected, with *Tyrobp* forming a major hub. Blue shading indicates the level of reduction of gene expression by 5B8 compared to IgG2b treatment. The thickness of the red border around the circles indicates the statistical significance of the differential expression, and the size of the circles indicates the number of connected genes in this co-expression network. Downregulated genes of interest were selected from those with $\log_2$ fold change of −0.5 or less and raw p-value < 0.05 (two-tailed moderated *t*-test). **b**, Mouse model of the human AD TYROBP network with data overlay of the 5B8-downregulated genes in the 5XFAD mice. Yellow-Blue gradient fill color indicates differential expression and red border thickness indicates significance of $P < 0.05$ (two-tailed moderated *t*-test).